Anisotropy of the momentum matrix element, dichroism, and conduction-band dispersion relation of wurtzite semiconductors

S. Shokhovets,[1,*] O. Ambacher,[2] B. K. Meyer,[3] and G. Gobsch[1]
[1]*Institute of Physics and Institute of Micro- and Nanotechnologies, Ilmenau University of Technology, Postfach 100565, 98684 Ilmenau, Germany*
[2]*Fraunhofer Institute for Applied Solid State Physics, Tullastrasse 72, 79108 Freiburg, Germany*
[3]*I. Physics Institute, Justus Liebig University, Heinrich-Buff-Ring 16, 35592 Giessen, Germany*
(Received 14 January 2008; revised manuscript received 11 May 2008; published 16 July 2008; corrected 5 August 2008)

By comparison of calculated imaginary parts of the ordinary and extraordinary dielectric functions of wurtzite semiconductors near the band gap with experimental results, we demonstrate that the interband matrix elements $E_P^{\parallel}$ and $E_P^{\perp}$ of the momentum operator parallel and perpendicular to the optic axis are different. $E_P^{\parallel}$ exceeds $E_P^{\perp}$ and their ratio increases along the series CdSe, CdS, ZnO. The *u* parameters of GaN, InN, and AlN suggest that the $E_P^{\parallel}/E_P^{\perp}$ ratio should increase along this series as well. We also determined the conduction-band dispersion relation and nonparabolicity, as well as the effective mass, as a function of electron concentration and wave vector for GaN, ZnO, CdS, and CdSe. In addition, optical response due to transitions into exciton-phonon complexes was observed and analyzed. We conclude that up to about ten phonons may participate in such absorption processes in ZnO.

DOI: 10.1103/PhysRevB.78.035207 PACS number(s): 71.20.Nr, 78.20.Ci, 78.20.Bh

I. INTRODUCTION

Due to the sixfold rotation symmetry of the crystal lattice, wurtzite semiconductors belong to a family of optically uniaxial crystals and should be characterized by two different sets of optical constants known as the ordinary $\varepsilon^{\perp}=\varepsilon_1^{\perp}+i\varepsilon_2^{\perp}$ and extraordinary $\varepsilon^{\parallel}=\varepsilon_1^{\parallel}+i\varepsilon_2^{\parallel}$ dielectric functions (DFs). This property is referred to as the optical anisotropy. The ordinary DF describes the propagation of light with the electric-field vector **E** perpendicular to the *c* (optic) axis (the ordinary wave), while the extraordinary DF refers to light with the **E** vector parallel to the *c* axis (the extraordinary wave). In the following, the *z* direction will be chosen as the direction of the optic axis, while the superscripts or subscripts $\perp$ and $\parallel$ will denote quantities related to the ordinary and extraordinary waves, respectively.

Provided the broadening of optical transitions is small enough, the optical anisotropy can be quite large in a spectral region of excitonic absorption because the oscillator strength of A, B, and C excitons strongly depends on the polarization of light, as shown in Table I for four wurtzite semiconductors, GaN, ZnO, CdS, and CdSe (see Sec. III for more details). Within the framework of the effective-mass approximation, in which the excitons are treated as being made up of an electron from the conduction band (CB) and a hole from each one (A, B, or C) of the three highest valence bands (VBs), this behavior is directly related to the symmetry character (p_x-, p_y-, or p_z-like) of the VB states close to the center of the Brillouin zone (BZ). Optical transitions involving the p_x- and p_y-like states are allowed for light polarized perpendicular to the *c* axis, while those involving the p_z-like states are allowed for light polarized parallel to the *c* axis.[4,5]

At a sufficient distance from the band gap, the optical anisotropy becomes significantly lower, as seen in Table I from experimental values of anisotropy parameters $\varepsilon_1^{\parallel}/\varepsilon_1^{\perp}$ (birefringence) and $\varepsilon_2^{\parallel}/\varepsilon_2^{\perp}$ (dichroism) for photon energies $E_{gA}-0.75$ eV and $E_{gA}+0.75$ eV, respectively, where E_{gA} is the energy gap between the CB and VB A. Generally, optical transitions over the whole spectral range contribute to $\varepsilon_1^{\perp}$ and $\varepsilon_1^{\parallel}$ values and, hence, to the magnitude of birefringence in the transparent region. For example for GaN, it was observed in Ref. 1 that the effect of high-energy critical points of the joint density-of-states function is considerably larger than that due to the E_0 critical point. On the other hand, owing to the resonant character of the imaginary part of the DF, its value at a photon energy *E* is determined by optical transitions only in a narrow range near the same photon energy provided the broadening of electronic states is not too large. In the present work, we analyze $\varepsilon_2^{\perp}(E)$ and $\varepsilon_2^{\parallel}(E)$ spectra up to a photon energy of about $E_{gA}+1.8$ eV, which is essentially below the E_1 critical point. In this spectral range, the imaginary part of the DF is determined by excitons at the fundamental absorption edge and band-to-band optical transitions between states of the three highest VBs and the lowest CB with electron wave vectors near the zone center. Then, a noticeably lower dichroism above the band gap compared to that due to exciton effects at the absorption edge (see Table I) may be qualitatively understood considering that, first, optical transitions from all three VBs to the CB contribute to ε_2 at a given photon energy and, second, there is a mixing of the VB states at nonzero wave vectors, giving rise to variations in transition probabilities.[6,7] For a quantitative description, explicit VB and CB dispersion relations must also be taken into account.[8] In addition, the hexagonal symmetry of wurtzite semiconductors allows the interband momentum matrix elements $E_P^{\perp}$ and $E_P^{\parallel}$ to be not equal,[9] which can also affect the optical anisotropy near the E_0 critical point.

As yet, no detailed physical model exists to account for the observed difference between the ordinary and extraordinary DFs above the band gap. It was derived from analysis of the conduction-band *g* factor[10] and band-structure calculations[11] that $E_P^{\parallel}$ is greater than $E_P^{\perp}$ in GaN. However, the opposite relationship has also been reported.[12] Both the

state mixing and noticeable anisotropy of the effective mass are present in the VB, as can be concluded from the reported parameters of the Rashba-Sheka-Pikus (RSP) Hamiltonian for GaN,[6,11,13–19] ZnO,[20,21] and CdS and CdSe.[14] Theoretical studies yield also different values of the electron effective mass parallel (m_{ez}) and perpendicular (m_{et}) to the c axis. However, no consensus exists on the relation between them, i.e., $m_{et}>m_{ez}$ was found for GaN,[6,11,15,18,19,22–27] ZnO,[22,27] and CdS and CdSe,[22] while other authors reported that $m_{et}<m_{ez}$ for GaN (Refs. 12, 13, 16, 28, and 29) and ZnO,[20] or $m_{et}\approx m_{ez}$ for GaN.[30–32] On the other hand, experiments revealed no detectable anisotropy of the CB for GaN (Ref. 33) and CdS and CdSe.[34] Only for ZnO, it was observed that $m_{et}>m_{ez}$ from cyclotron resonance[35] and infrared reflectance[36] measurements.

The goal of this work is to determine the interband momentum matrix elements of wurtzite semiconductors GaN, ZnO, CdS, and CdSe and to clarify based from these what physical properties are responsible for their dichroism near the E_0 critical point. We also observe the conduction-band nonparabolicity and determine the CB dispersion relation and effective mass. Our approach is based upon comparing experimental and calculated imaginary parts of the ordinary and extraordinary DFs. This work is an extension of our recent study of zinc-blende semiconductors[37,38] to the wurtzite crystal structure.

The paper is organized as follows: In Sec. II, modifications of the method to take into account the hexagonal crystal symmetry, as well as input parameters for the calculations of the DFs, are described. In Sec. III, we calculate the transition probability and study the effects of the band-structure anisotropy on the DF. It will be demonstrated that the experimentally observed dichroism near the E_0 critical point can be explained only by the assumption that $E_P^{\parallel}>E_P^{\perp}$. Section IV addresses experimental data for the DFs that we used to compare with the calculations. In particular, we re-examine existing literature data for ZnO, report on our measurements of C-plane ZnO crystals, and present a new data set which is in much better agreement with the $\mathbf{k}\cdot\mathbf{p}$ theory. In Sec. V, the concept of optical transitions into exciton-phonon complexes (EPC) is briefly discussed. It has been shown that the effect of EPC on the DFs is quite large in ZnO.[8] Here, we develop a model which takes into account differences in ionic character of the semiconductors investigated. In Sec. VI, main results of the present work are reported. We discuss the effect of dichroism near the E_0 critical point on birefringence in the transparent region and near the absorption edge. The determined anisotropy of the momentum matrix element is interpreted in terms of an inherent anisotropy of an ideal wurtzite structure and the departure of the actual crystal structure from the ideal wurtzite (Sec. VI A). The CB nonparabolicity and effective mass as a function of electron concentration and wave vector are presented and compared with those in literature in Sec. VI B, while in Sec. VI C a comparison to $\mathbf{k}\cdot\mathbf{p}$ models is done. Section VII is a brief summary of the results obtained.

II. MODEL AND INPUT PARAMETERS

Our model for calculating the imaginary part of the DF of zinc-blende cubic semiconductors in the vicinity of the direct band gap was introduced explicitly in Ref. 37. Contributions of optical transitions due to discrete exciton states and Coulomb-enhanced band-to-band (BB) transitions from three highest VBs to the CB are taken into consideration. As revealed by band-structure calculations, a feature specific for wurtzite semiconductors is a considerable splitting of each VB v (v=A, B, or C) into two different branches (sub-bands) $E_{v\sigma_v}(\mathbf{k})$ corresponding to two possible values, "+" or "−," of the spin variable σ_v that characterizes the VB eigenstates.[6,7] Another specific property of a hexagonal crystal is that, owing to the anisotropy of both the static dielectric constant and the reduced exciton mass, excitons no longer possess spherical symmetry and are elongated or flattened in shape. Within a simple anisotropic model,[39,40] the exciton energy levels are determined by the mean static dielectric constant $\varepsilon_s=(\varepsilon_s^{\perp}\varepsilon_s^{\parallel})^{1/2}$, the mean reduced exciton mass μ_0, and the anisotropy parameter γ. For the semiconductors in question, the anisotropy parameter is not large, and only small deviations from the hydrogenlike n^{-2} spectral law are observed.[40,41] Much more important corrections to the exciton binding energy and the hydrogenlike behavior originate in the coupling between exciton states belonging to different VBs, as well as in interactions of excitons with optical phonons.[20,42] However, since the exciton binding energy from experiments is taken and room-temperature data for the DF are analyzed in this work with a consequence that a noticeable broadening of optical transitions exists, we

TABLE I. Relative oscillator strength of excitons for two principal polarizations of light, as well as birefringence ($\varepsilon_1^{\parallel}/\varepsilon_1^{\perp}$) and dichroism ($\varepsilon_2^{\parallel}/\varepsilon_2^{\perp}$) at photon energies $E_{gA}-0.75$ eV and $E_{gA}+0.75$ eV, respectively.

	$\mathbf{E}\perp c$			$\mathbf{E}\parallel c$				
	A	B	C	A	B	C	$\varepsilon_1^{\parallel}/\varepsilon_1^{\perp}$	$\varepsilon_2^{\parallel}/\varepsilon_2^{\perp}$
GaN	1	0.619	0.381	0	0.763	1.237	1.032[a]	1.050[a]
ZnO	0.29	1	0.01	0.01	0	1.29	1.017[b]	1.096[b]
CdS	1	0.532	0.468	0	0.937	1.063	1.015[c]	1.084[c]
CdSe	1	0.374	0.626	0	1.251	0.749	1.016[c]	1.066[c]

[a]Reference 1.
[b]Reference 2.
[c]Reference 3.

expect that the hydrogenlike anisotropic model, as given by Eq. (2), is accurate enough to account for the excitonic contribution. Then, based on the results for zinc-blende cubic semiconductors[37,38] and taking into account the uniaxial optical anisotropy of wurtzite hexagonal semiconductors, the imaginary part of the DF at a photon energy E is expressed as follows:

$$\varepsilon_2^{\xi}(E) = f_x \varepsilon_{2\xi}^{\mathrm{DX}}(E) + \frac{A_0 m_0 E_P^{\xi}}{16\pi^2 E^2} \sum_{v,\sigma_v} \int_{\mathrm{BZ}} [1 + f_x(S_v - 1)] \times F_{v\sigma_v}^{\xi}(\mathbf{k}) \delta[E_c(\mathbf{k}) - E_{v\sigma_v}(\mathbf{k}) - E] d\mathbf{k}, \quad (1)$$

with

$$\varepsilon_{2\xi}^{\mathrm{DX}}(E) = \frac{A_0 m_0 E_P^{\xi}}{2E^2} \left(\frac{8\pi\varepsilon_0 \varepsilon_s}{e^2} \right)^3 \times \sum_v \sum_{n=1}^{\infty} F_{v\xi}^{\mathrm{DX}} \left(\frac{E_{bv}}{n} \right)^3 \delta\left(E - E_{gv} + \frac{E_{bv}}{n^2} \right), \quad (2)$$

and

$$S_v = (2\pi\sqrt{\varepsilon_v})/[1 - \exp(-2\pi/\sqrt{\varepsilon_v})], \quad (3)$$

where the first and the second terms in Eq. (1) describe contributions from discrete exciton states and BB transitions, respectively, ξ stands for $\perp$ or $\parallel$, f_x is the weighting factor for the excitonic contribution depending on the temperature and semiconductor of interest,[37,38] $A_0 = \hbar^2 e^2 / \varepsilon_0 m_0^2$, $\hbar$ is the Planck constant, e and m_0 are the free-electron charge and mass, respectively, ε_0 is the electric constant, E_P^{ξ} denotes the interband momentum matrix element in energy units, S_v is the Sommerfeld factor, $F_{v\sigma_v}^{\xi}(\mathbf{k})$ is a dimensionless wave-vector-dependent quantity that determines the transition probability between the σ_v sub-band of the VB v and the CB for the light polarization indicated by the superscript ξ, $E_c(\mathbf{k})$ is the dispersion relation in the CB, ε_s is the mean static dielectric constant, $F_{v\xi}^{\mathrm{DX}}$ and E_{bv} are the relative oscillator strength and the exciton binding energy of the exciton series belonging to the VB v, E_{gv} is the energy gap between the CB and the VB v at $\mathbf{k}=0$, and $\varepsilon_v = (E - E_{gv})/E_{bv}$.

The VB structure and transition probabilities were calculated by solving the RSP Hamiltonian for eigenfunctions and eigenvalues. The RSP Hamiltonian contains crystal-field (Δ_1) and spin-orbit (Δ_2, Δ_3) energies and seven A_i parameters. Our analysis of $\varepsilon_2^{\xi}(E)$ is restricted to a photon energy of about $E_{g\mathrm{A}} + 1.8$ eV, which corresponds to a limiting electron wave vector of approximately 3.5 nm^{-1}; i.e., $\mathbf{k}$ vectors up to about a quarter of the distance between the Γ point and the zone boundary are involved. This region near the zone center is well within the range of $\mathbf{k}$ points commonly employed for deriving the RSP parameters by a direct fitting to first-principles calculations of the VB structure.[6,13,14,19,20] The RSP parameters we use in the calculations are listed in Table II. To our knowledge, parameter sets presented by Jeon *et al.*[14] are the only ones available for CdSe and CdS. For ZnO, two sets of RSP parameters have been published.[20,21] We use the set in Ref. 20. Note that the values of crystal-field and spin-orbit splittings for CdSe, CdS, and ZnO quoted in Table II are close to those determined experimentally from low-temperature exciton absorption and reflectance measurements (see, e.g., Refs. 34 and 43).

TABLE II. Parameters of the Rashba-Sheka-Pikus Hamiltonian and room-temperature values of the electron effective mass, mean static dielectric constant, exciton binding energy, and weighting factor for the excitonic contribution to the DF used in calculations.

	GaN	ZnO	CdS	CdSe
Δ_1 (meV)	10.0	38.0	26.3	39.0
Δ_2 (meV)	6.2	−4.53	22.3	148
Δ_3 (meV)	5.5	−3.05	22.3	148
A_1	−6.75	−3.78	−4.53	−5.06
A_2	−0.592	−0.44	−0.39	−0.43
A_3	6.20	3.45	4.02	4.50
A_4	−2.83	−1.63	−1.92	−1.29
A_5	−2.90	−1.68	−1.92	−1.29
A_6	−3.80	−2.23	−2.59	−0.467
A_7 (eV Å)	0.0801	0.180	0	0
m_{e0}^*	0.183	0.216	0.178	0.118
ε_s	9.60	7.93	8.53	9.34
E_b (meV)	23.6	54	26.5	13.9
f_x	0.97	0.93	0.78	0.53

Much theoretical work was done in deriving the VB parameters of GaN.[6,11,13–19] However, the calculated crystal-field and spin-orbit splittings deviate significantly from values observed by experiments. The crystal-field splitting Δ_1 especially is strongly overestimated by most calculations; see, e.g., the lists in Refs. 44 and 45. A consistent set of VB parameters for GaN is not available at present.[33] It must be emphasized that, owing to the small spin-orbit and crystal-field splittings, their experimentally determined values tend to be more reliable than those from calculations. On the other hand, a direct fitting to band-structure calculations is at present the only way to obtain all A_1-A_7 parameters. To our knowledge, only Torii *et al.*[46] reported on the experimental determination of several A_i parameters from reflectance and emission of excitonic polaritons. However, the reported set is incomplete and, additionally, depends on the electron effective mass chosen. The set used in this work (see Table II) is composed as follows: We employ the crystal-field and spin-orbit energies resulted from a comprehensive study of excitons in epitaxial GaN films by Gil.[47] Note that these Δ_i's describe not only the energy positions of A, B, and C excitons but also their relative intensities. In particular, the calculated relative oscillator strengths for the $\mathbf{E} \perp c$ polarization (see Table I) are in good agreement with experimental polarizabilities of the excitons observed with homoepitaxial GaN films.[48] However, using the Δ_i values from experiments needs the A_7 parameter to be modified properly. Because a major difference between calculations and experiments is the crystal-field energy Δ_1 and the quantity $2(A_7^2/\Delta_1)$ affects the effective mass at the Γ point,[6,13] we evaluated the average of $2(A_7^2/\Delta_1)$ terms reported in the literature.[6,11,13,15,17–19] Combining it with the Δ_1 value from Table II yields the A_7 parameter. At large wave vectors, when the spin-orbit splitting and terms linear in $\mathbf{k}$ in the RSP Hamiltonian may be ignored

(i.e., $\Delta_2=\Delta_3=0$, $A_7=0$), all three VBs are parabolic in directions perpendicular and parallel to the optic axis. Within this approximation, the effective mass (in units of the free-electron mass) is as follows:[13]

$$1/m^*_{At} = -(A_2 + A_4 - A_5),$$

$$1/m^*_{Bt} = -(A_2 + A_4 + A_5),$$

$$1/m^*_{Ct} = -A_2,$$

$$1/m^*_{Az} = 1/m^*_{Bz} = -(A_1 + A_3),$$

$$1/m^*_{Cz} = -A_1.$$

Parameters A_1–A_5 listed in Table II were derived by averaging the above effective masses reported in Refs. 6, 11, and 13–19, while A_6 was then deduced using the quasicubic model.[6]

Further parameters needed to calculate ε_2^ξ by using Eqs. (1)–(3) are the electron effective mass, the mean static dielectric constant, the exciton binding energy, and the weighting factor for excitonic contribution. It was mentioned in Sec. I that except for ZnO, experiments indicate no or negligible CB anisotropy. Furthermore, we will demonstrate by calculations in Sec. III that a moderate CB anisotropy would have only little effect to be not enough to account for the experimentally observed optical anisotropy. For these reasons, we adopt a spherical CB. The electron effective mass at the CB bottom used in our calculations is given in Table II. The values for CdSe and CdS stem from recent cyclotron resonance measurements,[49] while those for ZnO and GaN were obtained in this work (see Sec. VI).

The assumption of a spherical CB allows us to use a simple description of the nonparabolicity, as in Refs. 37 and 38, with nonparabolicity coefficients N_i which do not depend on the direction in **k** space:

$$E_c(\mathbf{k}) = \frac{\hbar^2}{2m_0}\frac{\mathbf{k}^2}{m^*_{e0}} + \sum_{i=1}^{i_0} N_i \left(\frac{\mathbf{k}^2}{m^*_{e0}}\right)^{i+1}, \tag{4}$$

where m^*_{e0} is the electron effective mass at the CB bottom in units of the free-electron mass and the electron energy is counted from the CB bottom. Then, the energy-dependent electron effective mass m^*_e can be introduced by the following equations:

$$E_c = \frac{\hbar^2 k^2}{2m_0 m^*_e}, \quad m^*_e = m^*_{e0}\left(1 + \sum_{j=1}^{j_0} M_j E_c^j\right), \tag{5}$$

where M_j is a new set of nonparabolicity coefficients. Also the momentum (dynamical) electron effective mass m_p, defined by $1/m_p=(1/\hbar^2 k)(dE_c/dk)$, can be found as a function of electron energy and concentration n_e (see Ref. 38 for more details).

To deduce room-temperature ε_s^ξ values, we used the Lyddane-Sachs-Teller relation $\varepsilon_s^\xi=\varepsilon_\infty^\xi(\omega_{\mathrm{LO}}^\xi/\omega_{\mathrm{TO}}^\xi)^2$, which may be written independently for the two principal polarization directions in hexagonal crystals,[50] where ε_∞^ξ is the high-frequency dielectric constant, while ω_{LO}^ξ and ω_{TO}^ξ are frequencies of the LO and TO phonons polarized perpendicular ($\xi=\perp$) and parallel ($\xi=\parallel$) to the optic axis. These phonon polarizations are also known as E_1 and A_1 modes, respectively. Values of ε_∞^ξ were taken from spectroscopic ellipsometry measurements of GaN (Ref. 1) and studies of ZnO, CdS, and CdSe by prism-minimum-deviation method.[51–53] Frequencies of E_1 and A_1 optical phonons were obtained by averaging Raman,[54–59] infrared reflectance,[60] and infrared spectroscopic ellipsometry[61] data for GaN, Raman,[62–65] infrared reflectance,[36] and infrared spectroscopic ellipsometry[65] data for ZnO, as well as Raman and infrared spectroscopy data for CdS and CdSe compiled in Ref. 34. Values of ε_∞^ξ and ε_s^ξ derived in this way agree well with data from infrared reflectance and transmission studies of GaN,[58,66] ZnO,[67] CdS,[68,69] and CdSe,[68,70] from prism-coupled-waveguide measurements for GaN (Ref. 71) and ZnO,[72] and from spectroscopic ellipsometry for ZnO.[65,73] The resultant mean dielectric constants $\varepsilon_s=(\varepsilon_s^\perp \varepsilon_s^\parallel)^{1/2}$ are listed in Table II.

The exciton binding energy is mostly known from low-temperature experiments. Usually somewhat differing values are reported for A, B, and C excitons (see Refs. 74–77 for GaN, Refs. 78–84 for ZnO, and Ref. 34 for CdS and CdSe). However, noticeable discrepancies exist between data of various groups, especially for ZnO. Calculations of excitonic spectra from first principles yielded similar binding energies of the A, B, and C, excitons for GaN (Ref. 85) and ZnO.[86] In this work the exciton binding energy is taken to be identical for all three excitons. Its average values at low temperatures are 26 meV for GaN,[42,74–77,87,88] 59 meV for ZnO,[5,20,78–84,89] 29.1 meV for CdS,[34,90,91] and 15.4 meV for CdSe.[34] Considering the temperature dependence of the static dielectric constant reported in Refs. 92–95 and using the procedure described in Refs. 37 and 38, we obtained the room-temperature E_b values presented in Table II.

The weighting factor f_x for ZnO, CdS, and CdSe was calculated using Eq. (16) of Ref. 37. The necessary experimental data were taken from Ref. 34. For GaN, f_x was set at 0.97.[37] This value agrees well with recent experimental data on elastic constants,[58,96] heat capacity,[97–100] thermal conductivity,[97,99–101] and phonon mean free path.[100]

III. TRANSITION PROBABILITY AND EFFECTS OF THE BAND-STRUCTURE ANISOTROPY

In calculating the VB structure and the transition probability between the VB and the CB, we follow Sirenko *et al.*[7] (see also Ref. 37). By applying six basis functions $|v_l,\sigma_v\rangle$, where $l=1-3$, the 6×6 RSP Hamiltonian is transformed into the block-diagonal form, with the spin variable $\sigma_v=\pm$ assigning the basis states to the 3×3 upper (H_+) and lower (H_-) Hamiltonian blocks [see Eqs. (21) and (22) of Ref. 7]. The eigenstate belonging to the σ_v sub-band of the VB v is characterized by the eigenfunction $w_{v\sigma_v}$ which is a linear combination of $|v_l,\sigma_v\rangle$:

$$w_{v\sigma_v} = \sum_{l=1}^{3} (a_{vl\sigma_v} + ib_{vl\sigma_v})|v_l,\sigma_v\rangle. \tag{6}$$

Solving the H_+ and H_- matrices yields the eigenfunctions $w_{v\sigma_v}(\mathbf{k})$ and eigenvalues $E_{v\sigma_v}(\mathbf{k})$ for the "upper" (corre-

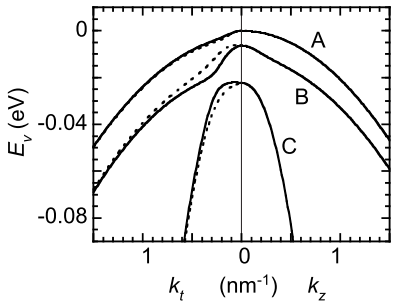

FIG. 1. Valence-band structure of GaN calculated using RSP parameters of Table II. Upper and lower sub-bands are shown by the solid and dotted lines, respectively.

sponding to $\sigma_v=+$) and "lower" ($\sigma_v=-$) sub-bands of each VB v.

An electron state in the CB is described by a Bloch function $u_{c\sigma_c}$, where σ_c denotes the electron spin. In the dipole approximation, the transition probability is determined by the matrix element $\langle w_{v\sigma_v}|\mathbf{ep}|u_{c\sigma_c}\rangle$, where $\mathbf{e}$ is the unit vector in direction of the light polarization and $\mathbf{p}$ is the momentum operator. To calculate the above matrix element, we used matrix elements $\mathbf{ep}_{l\sigma_v\to c\sigma_c}=\langle v_l,\sigma_v|\mathbf{ep}|u_{c\sigma_c}\rangle$ of optical transitions between valence-band basis states and conduction-band states given in Table 1 of Ref. 7. As similarly done in Ref. 37, we introduce the squared total matrix element $(|\mathbf{ep}_{vc}|^2_{\mathrm{tot}})_{\sigma_v}$ defined as a noncoherent sum over two possible sets of spin configurations due to the twofold spin degeneracy of the CB:

$$(|\mathbf{ep}_{vc}|^2_{\mathrm{tot}})_{\sigma_v}=\sum_{l=1}^{3}(a^2_{vl\sigma_v}+b^2_{vl\sigma_v})|\mathbf{ep}_{l\sigma_v\to c\sigma_c}|^2. \tag{7}$$

Equation (7) describes the transition probability between the σ_v sub-band of the VB v and the CB for an arbitrary polarization of light. The latter is specified by the direction of the $\mathbf{e}$ vector characterized by spherical angles θ_e and φ_e. Due to rotation symmetry of the RSP Hamiltonian, the transition probability does not depend on φ_e.[7] Setting $\theta_e=\pi/2$ and $\theta_e=0$ in Eq. (7) yields the transition probability for the ordinary and extraordinary waves, respectively. For the two principal light polarizations, Eq. (7) can be rewritten as follows:[37,102]

$$(|\mathbf{ep}_{vc}|^2_{\mathrm{tot}})^{\xi}_{\sigma_v}=\frac{m_0}{2}E^{\xi}_P F^{\xi}_{v\sigma_v}(\mathbf{k}), \tag{8}$$

where $E^{\xi}_P\equiv(2m_0/\hbar^2)|P_\xi|^2$, P_ξ is the Kane parameter and a dimensionless quantity $F^{\xi}_{v\sigma_v}(\mathbf{k})$ describes the wave-vector dependence of the transition probability between the sub-band σ_v of the VB v and the CB. Note that the momentum matrix element E^{ξ}_P is a materials constant which, as seen from Eqs. (1)–(3), scales the magnitude of the imaginary part of the DF, while the spectral dependence of $\varepsilon^{\xi}_2(E)$ is determined by details of the band structure and the quantity $F^{\xi}_{v\sigma_v}(\mathbf{k})$. The latter will further be called the relative transition probability.

Figure 1 presents the VB structure of GaN in the direction

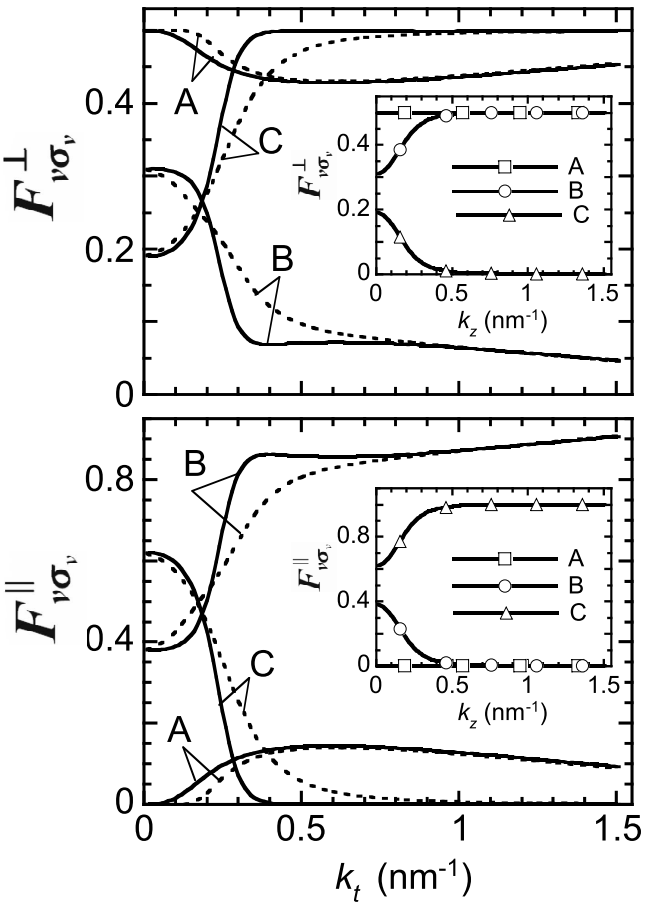

FIG. 2. Relative transition probability between the valence bands and the conduction band of GaN for ordinary (top) and extraordinary (bottom) waves involving states with wave vector perpendicular to the optic axis. The solid and dotted lines refer to upper and lower sub-bands, respectively. The insets show the results for states with wave vector parallel to the optic axis.

perpendicular (k_t) and parallel (k_z) to the c axis calculated using the composite set of RSP parameters (see Table II). Constant-energy surfaces of all six sub-bands are rotationally symmetric [for their constant-energy contours, see the inset of Fig. 3 (top)]. The two sub-bands of each one of the three VBs are degenerate when $\mathbf{k}$ is parallel to the c axis. As the $\mathbf{k}$ direction moves away from the optic axis, the splitting of the sub-bands increases and reaches a maximum for an in-xy-plane orientation of the wave vector. In Fig. 2, the relative transition probability for the ordinary and extraordinary waves is shown as a function of the wave-vector length for states with $\mathbf{k}$ perpendicular to the optic axis. Major changes occur in the vicinity of the anticrossing point of the B and C VBs (compare to Fig. 1). The insets of Fig. 2 present the transition probability for states with $\mathbf{k}\|c$. Comparison to the respective data for $\mathbf{k}\perp c$ orientation reveals that, generally, there is a strong dependence on the angle θ between the wave vector $\mathbf{k}$ and the optic axis. A qualitatively similar behavior is observed for other semiconductors studied as well. Some peculiarities of ZnO are related to the anomalous valence-band ordering.[5,20] However, this has no fundamentally different effect on the DFs, as revealed by the

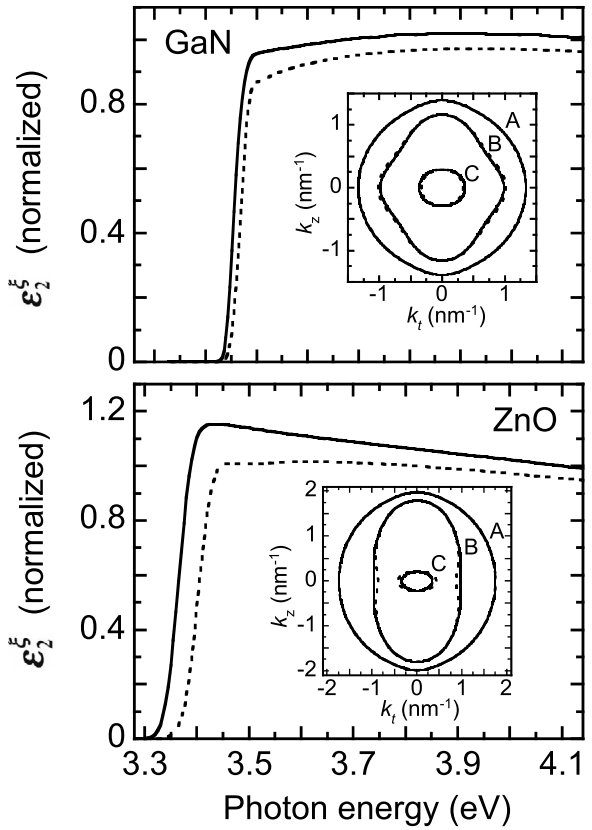

FIG. 3. Normalized ordinary (solid) and extraordinary (dotted) imaginary parts of the dielectric functions of GaN (top) and ZnO (bottom) due to band-to-band optical transitions. The insets show constant-energy contours of the valence bands in a plane containing the optic axis (solid and dotted lines for upper and lower sub-bands, respectively; E_v=0.04 eV from top of the A band).

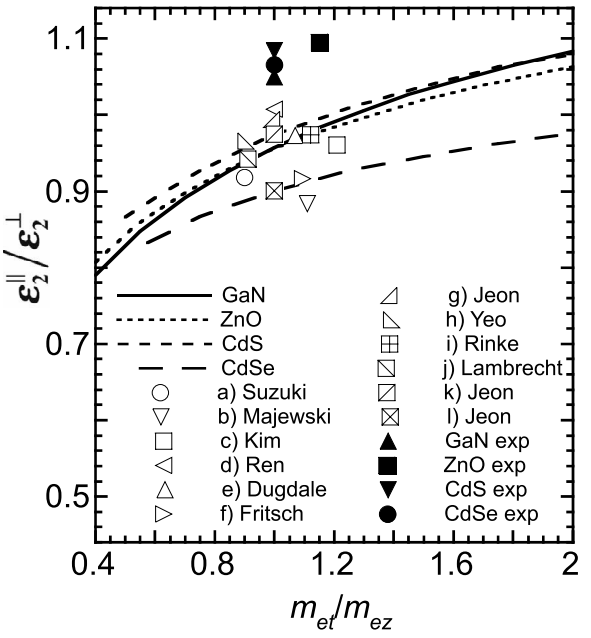

FIG. 4. Dichroism at a photon energy E_{gA}+0.75 eV. The filled symbols denote experimental data for GaN (Ref. 1), ZnO (Ref. 2), CdS, and CdSe (Ref. 3). The lines represent the dependence on m_{et}/m_{ez} ratio calculated using RSP parameters in Table II. The open symbols are data points obtained with original RSP parameters and electron effective masses proposed in the literature for GaN [(a)–(i)], ZnO (j), CdS (k), and CdSe (l). For the calculations, $E_P^\parallel = E_P^\perp$ was assumed. (a) Ref. 13; (b) Ref. 15; (c) Ref. 6; (d) Ref. 17; (e) Ref. 18; (f) Ref. 19; (g) Ref. 14; (h) Ref. 16; (i) Ref. 11; (j) Ref. 20; [(k) and (l)] Ref. 14.

calculations, and will be not discussed in detail.

As seen in Fig. 2, for small **k** the probabilities of optical transitions involving A, B, and C valence-band states are approximately independent of θ and wave-vector length. The sum $F_v^\xi(\mathbf{k}) = F^\xi_{v,\sigma_v=+}(\mathbf{k}) + F^\xi_{v,\sigma_v=-}(\mathbf{k})$ at $\mathbf{k}=0$ determines the oscillator strength of the respective excitons in both principal light polarizations, i.e., $F^{DX}_{v\xi} = F^\xi_v(0)$ in Eq. (2). Note also that the equality $\Sigma_v F^\xi_v(0) = 2$ holds regardless of the polarization of light. $F^{DX}_{v\xi}$ values for GaN, CdS, and CdSe that resulted from the RSP parameters in Table II are listed in Table I. For ZnO, modified values are given which account for the experimentally observed weakness of the A exciton (see Sec. VI for a detailed discussion).

Further, we will address features of the band structure that affect the dichroism of wurtzite materials in a spectral region above the band gap, where the BB transitions dominate. For these calculations, $E_P^\perp = E_P^\parallel$ is assumed. Figure 3 shows the imaginary part of the ordinary and extraordinary DFs of GaN and ZnO due to transitions between all three VBs and the CB. The Coulomb enhancement and broadening (see Table VI for the broadening parameter) are included. The RSP parameter sets of Table II are used and a parabolic and isotropic CB is assumed. The spectra are normalized on $\varepsilon_2^\perp$ values at the photon energy E_{gA}+0.75 eV. Two important features should be emphasized which are a direct consequence of the hexagonal symmetry of wurtzite semiconductors. First, the onset of a strong absorption of the extraordinary wave is shifted to higher photon energies compared to the ordinary wave. This behavior correlates with the polarization dependence of excitonic absorption. The explanation is that at small wave vectors, the probabilities of BB transitions involving the A, B, and C VBs only weakly depend on **k**, being approximately the same as for the respective excitons, as seen from Fig. 2. Second, as the wave vector is increased, strong state mixing and related changes in the transition probabilities occur. This, however, does not completely eliminate the difference between $\varepsilon_2^\perp$ and $\varepsilon_2^\parallel$; their magnitudes remain unequal at larger photon energies as well. Such a dependence on the light polarization is not observable in cubic zinc-blende semiconductors.[37]

As for the magnitude of dichroism above the band gap, we see from Fig. 3 that $\varepsilon_2^\parallel/\varepsilon_2^\perp < 1$ (this is also valid for CdS and CdSe), whereas the opposite relationship is observed by experiments (see Table I). However, the calculations show that the $\varepsilon_2^\parallel/\varepsilon_2^\perp$ ratio depends on both the CB anisotropy and an individual set of RSP parameters. The effect of the CB anisotropy was studied assuming a parabolic CB with an ellipsoidal constant-energy surface characterized by components m_{et} and m_{ez} of the electron effective mass tensor. The components were chosen to satisfy the requirement $m^*_{e0} = (m^2_{et} m_{ez})^{1/3}/m_0$, where m^*_{e0} is taken from Table II. In Fig. 4, the calculated dichroism at E_{gA}+0.75 eV is presented as a

function of m_{et}/m_{ez} ratio for GaN, ZnO, CdS, and CdSe provided $E_P^{\perp}=E_P^{\parallel}$ and RSP sets of Table II are used. As seen, the $\varepsilon_2^{\parallel}/\varepsilon_2^{\perp}$ ratio increases with increasing m_{et}/m_{ez} value. However, the effect is relatively weak, not enough to explain the experimentally observed dichroism (filled symbols in Fig. 4). Open symbols refer to the calculations employing original RSP parameters and electron effective masses proposed in the literature.[6,11,13–20] More or less elongated and warped constant-energy surfaces of the VBs (see the insets of Fig. 3) are obtained according to various authors. As a result, scattering of the calculated data points is observed (see Fig. 4). For example, a larger elongation of the B and C VBs in the direction parallel and perpendicular to the optic axis, respectively, promotes a lesser $\varepsilon_2^{\parallel}/\varepsilon_2^{\perp}$ value. However, the elongation is not the only deciding factor. Both the transition probability and the detailed shape of the constant-energy surfaces are sensitive to all Δ_i and A_i parameters, and the resultant dichroism is determined by their interplay.

The following conclusions can be drawn from the above discussion, especially from Figs. 3 and 4. First, the experimentally observed dichroism cannot be explained quantitatively without an assumption that $E_P^{\parallel}>E_P^{\perp}$. Second, the CB of CdSe and CdS is isotropic,[34] while m_{et}/m_{ez} values for GaN and ZnO reported from calculations[6,11–32] and experiments[33–36] fall into an interval of about 0.8–1.2. Such a moderate CB anisotropy would only slightly alter the dichroism calculated for $m_{et}/m_{ez}=1$ (see Fig. 4). Therefore, we will adopt an isotropic but not parabolic CB in the following analysis for all semiconductors studied.

IV. EXPERIMENT

Jellison and Boatner[2] determined the ordinary and extraordinary DFs of ZnO by generalized ellipsometry. Their data are, perhaps, the most accurate in the region close to the band gap. The measurements were performed with high spectral resolution on samples grown using the chemical vapor transport method and the hydrothermal method, undoped and Sn doped, with in-plane and off-normal orientations of the optic axis. Near and above the band edge, the resulting DFs from all samples were identical within error, while the refractive indices determined below the band edge agree with those by prism-minimum-deviation method. However, an unexpected lowering of the ε_2 magnitude is observable at photon energies higher than 4 eV. Using the data in Ref. 2 results in a low CB nonparabolicity,[8] which contradicts the $\mathbf{k}\cdot\mathbf{p}$ theory. This discrepancy may be related to the overestimation of the overlayer thickness d_{ovr} which was derived in Ref. 2 under the assumption that the overlayer causes all experimentally observed deviations from an ideal behavior expected for an abrupt air/ZnO boundary in the transparent region (1.5–3.1 eV). Then, the fitting parameters of the overlayer were used to determine the optical constants of ZnO above the band gap (up to 5 eV). However, ellipsometric data can be affected not only by an overlayer but also by other effects, such as backside reflection and light scattering, which may be especially strong in a transparent region. In addition, as the effect of an overlayer is proportional to $(d_{\mathrm{ovr}}/\lambda)^2$, where λ is the wavelength of the light,[103] an error

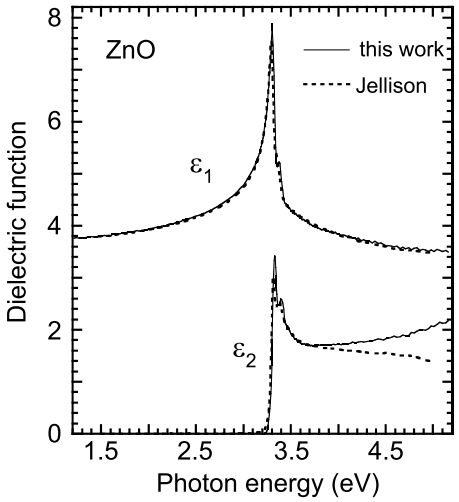

FIG. 5. Isotropic dielectric function of ZnO measured in this work (solid lines) in comparison to the ordinary DF from Ref. 2 (dotted lines).

in d_{ovr} that is not important at low photon energies may become significant at higher energies. Therefore, more reliable optical constants would result if (a) detrimental effects due to nonidealities of samples are minimized and (b) a self-consistent procedure of data analysis is used, e.g., multiple-sample fit in which many data sets are treated simultaneously in the same spectral range.

To reduce backside-reflection and light-scattering effects, we carried out measurements with the sample surface to be screened off except for a small active area. Four different *C*-plane wafers, one-side polished, supplied by Tokyo Denpa Co., Ltd. (hydrothermal method), Eagle-Picher Co., Ltd. (vapor-phase method), Cermet, Inc. (pressurized melt growth technique), and CrysTec GmbH (hydrothermal method) were studied using spectroscopic ellipsometry (angles of incidence of 55°, 60°, 65°, and 70°) and reflectance (*s*-polarized light, angles of incidence of 20° and 40°). From measurements of the *C* plane above the absorption edge, the so-called isotropic DF is determined.[1,104] This was derived by multiple-sample fit to all the spectra measured. In doing that, the material properties were assumed to be identical for all samples, while the overlayer thickness was allowed to vary for different samples. The overlayer was modeled using a 50%/50% air/ZnO Bruggeman effective medium. The result is presented in Fig. 5, together with the ordinary DF from Ref. 2. Note distinctions between the ordinary DF and the "isotropic" DF observable in the region of excitonic absorption. A detailed discussion of the relation between the ordinary, extraordinary, and isotropic DFs is out of the scope of this work and will be done elsewhere. Here we only remark that, owing to considerably larger exciton binding energy, oscillator strength and energy separation between the (A, B) exciton doublet and the C exciton, these distinctions are much more important for ZnO than for GaN, in agreement with our model calculations (not presented here). At a sufficient distance from the absorption edge, approximately equal (within less than 2%) imaginary parts of the ordinary and isotropic DFs are predicted by the calculations for ZnO. Within experimental error, this is also fulfilled, as seen in

Fig. 5, except for photon energies higher than 3.7 eV, where our ε_2 data significantly deviate from that of Ref. 2. We attribute this discrepancy to an overestimated overlayer thickness in Ref. 2, as discussed above. Therefore, in determining the momentum matrix elements and the CB nonparabolicity of ZnO, we used a compiled data set consisting of $\varepsilon_2^{\perp}$ and $\varepsilon_2^{\parallel}$ data of Ref. 2 in the 3.1–3.7 eV region and our data for $\varepsilon_2^{\perp}$ at higher photon energies.

So far, no experimental data for the ordinary and extraordinary DFs of GaN close to and above the band gap are available in the literature. However, the isotropic DF is known with good accuracy from measurements of *C*-plane films. Here, we use our data presented in Ref. 104 which were obtained from spectroscopic ellipsometry study of high-quality films with low electron concentration grown on *C*-plane sapphire substrates. The room-temperature isotropic ε_2 value of GaN is close to the imaginary part $\varepsilon_2^{\perp}$ of the ordinary DF over the whole spectral range studied.[104] Subtle distinctions occur only near the main excitonic peak.

There have been several spectroscopic ellipsometry studies of CdS (Refs. 105 and 106) and CdSe.[107–109] In this work, we use data sets published by Ninomiya and Adachi,[106,109] which, to our knowledge, are the only complete ones for the both light polarizations in a spectral range close to and above the absorption edge. Single crystals grown by a vapor-phase method, not intentionally doped, with in-plane orientation of the *c* axis were measured. Possible effects of the overlayer due to surface roughness and contaminations have been not completely clarified and not eliminated, with a consequence that an overestimated ε_2 magnitude in data sets of Refs. 106 and 109 may be expected. This, however, should have little effect on the $E_P^{\parallel}/E_P^{\perp}$ ratio determined in this work.

V. EXCITON-PHONON COMPLEXES

Owing to the small energy separation between A and B excitons in GaN and ZnO, they are not resolved in room-temperature absorption, reflectance, and spectroscopic ellipsometry spectra; a single peak is observed due to the both excitons in the $\mathbf{E}\perp c$ polarization.[2,104] A similar peak seen in the $\mathbf{E}\parallel c$ polarization is shifted to a higher photon energy and is related to the *C* exciton. In addition, a significantly broader and asymmetrical band is present on the high-energy side for the both light polarizations.[2] Studying the transmission of ZnO crystals, Liang and Yoffe[78] first suggested that these sidebands are due to transitions into exciton-phonon complexes (EPCs). An additional broad feature which appears at about one LO-phonon energy above the main excitonic peak has been observed by many other authors in the optical spectra of GaN,[110,111] ZnO,[112,113] CdS and CdSe,[114] and other materials.[115,116] It can be concluded from experiments that EPC transitions are favored in materials of increasing ionic character, where the lattice can be readily polarized. In addition, the energy of the complexes is not a simple sum of the exciton and phonon energies, and more than one phonon may be involved.

The problem of the optical response including processes where a photon simultaneously creates an exciton and phonons was treated theoretically in Refs. 116–119. However, there is yet no analytical expression available for the description of EPC. In Ref. 8, a simple model was used which accounts for the sidebands in spectra of the ordinary and extraordinary DFs of ZnO as phonon replicas of the discrete exciton contribution. It was found that EPCs make a significant contribution to the DFs and might not be neglected in quantitative analyzing of experimental data. Here, we develop a more sophisticated model to take into consideration differences in the ionic character of the semiconductors studied. To provide an insight into properties of EPC, below we briefly discuss some basic results regarding electron-phonon and exciton-phonon systems.

In a polar semiconductor, a moving electron interacts with the positive and negative lattice ions displaced by the own electric field of the electron. The state of the electron with its surrounding polarization of the crystal lattice can be thought a quasiparticle, the polaron. In theory, the polaron is described as an electron surrounded by a cloud of virtual phonons.[120] The interaction with the lattice via LO phonons is dominant. This coupling is described by a Fröhlich Hamiltonian with a dimensionless (Fröhlich) parameter $\alpha_{e,h}$ that plays the role of a coupling constant of the charged particle (electron or hole) with the lattice:

$$\alpha_{e,h} = \frac{e^2}{8\pi\varepsilon_0\hbar}\left(\frac{2m_{e,h}}{\hbar\omega_{\mathrm{LO}}}\right)^{1/2}\left(\frac{1}{\varepsilon_\infty}-\frac{1}{\varepsilon_s}\right), \tag{9}$$

where the subscripts *e* and *h* refer to the electron polaron and the hole polaron, respectively, and $m_{e,h}$ is the bare effective mass of the charged particle. It was shown[120] that the mean number of phonons in the cloud around the charged particle is $N_{e,h}=\alpha_{e,h}/2$, and the induced polarization charge distribution has a mean extension of $r_{e,h}=(\hbar/2m_{e,h}\omega_{\mathrm{LO}})^{1/2}$, known as the polaron radius. Values of the polaron radii are especially important for an exciton-phonon system.[121,122] As the distance between the electron and the hole is decreased, their polarization clouds partially neutralize each other. It allows two limiting cases to be treated: (a) when the exciton radius a_x is larger than the sum of the polaron radii, the exciton can be assumed to consist of two independent polarons; and (b) for small a_x, the exciton is coupled as a whole to the crystal lattice. In the former case, the limiting number of phonons coupled to the exciton is $N=(\alpha_e+\alpha_h)/2$, while no phonons couple to the exciton if its radius is very small compared to the polaron radii.[121]

In Table III, exciton and polaron radii and Fröhlich parameters are presented, as well as quantities used to calculate them: $\varepsilon_\infty=(\varepsilon_\infty^{\perp}\varepsilon_\infty^{\parallel})^{1/2}$; LO-phonon energy $\hbar\omega_{\mathrm{LO}}$, where $\omega_{\mathrm{LO}}=(\omega_{\mathrm{LO}}^{\perp}\omega_{\mathrm{LO}}^{\parallel})^{1/2}$; and the hole effective mass m_h^*. The latter was evaluated as the average of the effective masses for all three VBs at $\mathbf{k}=0$ in two principal directions. ε_s values are given in Table II. As seen from Table III, the exciton radius is in the order of the sum of the polaron radii, and the sum of Fröhlich parameters for electrons and holes is quite large. Hence, especially for ZnO, a considerable number of phonons are expected to couple with excitons. Recently, using Monte Carlo method, Mishchenko *et al.*[123] studied the structure of the polaron cloud in terms of partial contributions of states with $N=0$, 1, 2, 3, etc., phonons. According to

TABLE III. Mean values of high-frequency dielectric constant, LO-phonon energy, and hole effective mass, as well as exciton and polaron radii, Fröhlich coupling constants, and parameters of exciton-phonon complexes (see text).

	GaN	CdSe	CdS	ZnO
ε_∞	5.25	6.00	5.24	3.65
$\hbar\omega_{LO}$ (meV)	91.5	26.1	37.6	72.0
m_h^*	0.611	0.835	0.780	1.374
a_x (nm)	3.18	5.54	3.18	1.66
r_e (nm)	1.51	3.65	2.44	1.59
r_h (nm)	0.826	1.32	1.14	0.621
α_e	0.450	0.451	0.576	0.930
α_h	0.824	1.24	1.23	2.38
f_0	0.12	0.15[a]	0.16[a]	0.31
b	0.25	0.29[a]	0.30[a]	0.67
F_{EPC}	0.16	0.21[a]	0.23[a]	0.99
$\Delta E_0/(\hbar\omega_{LO})$	0.96	0.86[a]	0.82[a]	0.43

[a]Obtained by linear interpolation between GaN and ZnO.

their results, for $\alpha_e=1$ these contributions are about 0.6, 0.3, 0.08, and 0.015 for the first four states. As α_e is increased, the contribution of the $N=0$ state decreases. For example, it amounts to only 0.17 for $\alpha_e=3$. In addition, a peak at $\bar{N} \geq 1$ arises. The distribution of multiphonon states around the peak is asymmetric with a tail on the $N>\bar{N}$ side.

Based on these results and on our previous study,[8] we modeled the effect of EPC on the DF as multiphonon ($N=1,2,3,\ldots,N_m$) replicas of the discrete excitonic contribution scaled by a factor $f_0 b^{N-1}$ and shifted to higher photon energies by $N\Delta E_0$. Then, a quantity $F_{EPC}=f_0\Sigma_{N=1}^{N_m} b^{N-1}$ is a measure of the EPC contribution as compared to that of the discrete excitons, with f_0 yielding the relative contribution of the $N=1$ state. On condition that b is less than unity, which should be expected for the semiconductors studied, a larger b will result in a more asymmetrical sideband. Values of f_0, b, and ΔE_0 were treated as adjusted parameters to be determined from comparison with experiment.

Figure 6 shows room-temperature experimental data (circles) for the DF of ZnO (Ref. 2) and GaN.[104] Note the presence of the sidebands in the spectra of both materials at photon energies above the excitonic peaks, with the GaN sideband being much less pronounced than the ZnO ones. The solid lines in Fig. 6 represent fits to the experimental data, taking into account the Coulomb-enhanced BB transitions and discrete excitons, as specified by Eqs. (1)–(3), as well as the EPC, as described above. Their particular contributions are shown by broken lines. It is seen in Fig. 6 that the sidebands cannot be reproduced correctly without taking into consideration the presence of EPC.

Table III lists parameters that describe the contribution of EPC to the DFs. Other results of fits will be presented in Sec. VI. Below we give brief explanations to the derived parameters of EPC. Provided that $(\alpha_e+\alpha_h)\approx 1$, $b=0.25$ can be adopted from the data of Ref. 123. This was found to be appropriate for GaN and means that states with $N>3$ are practically not present in the polarization cloud around the

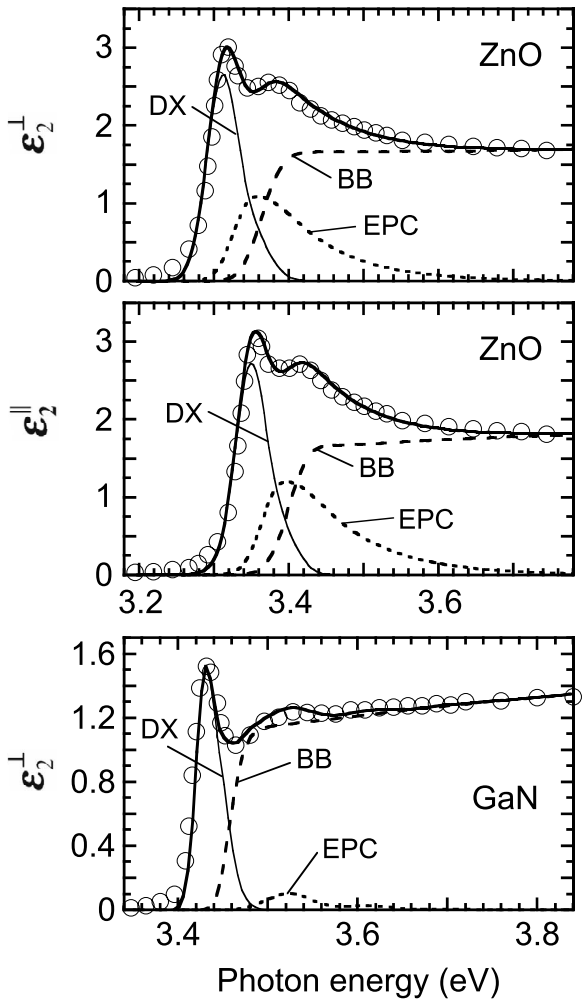

FIG. 6. Experimental DFs (circles) of ZnO (Ref. 2) and GaN (Ref. 104) and fits (solid lines). Contributions of free excitons, band-to-band transitions, and transitions into exciton-phonon complexes are denoted by DX, BB, and EPC, respectively.

excitons. For ZnO, a significantly larger b value was determined from the fits (see Table III) indicating that states up to $N_m=12$ can be effective. In addition, the determined f_0 value is considerably larger for ZnO than for GaN. The resulting F_{EPC} values, which characterize the magnitude of the EPC contribution as compared to that of the discrete excitons, are also shown in Table III. As seen, contributions of discrete excitons and EPC have the same order in the case of ZnO. For GaN, the effect of EPC is of lesser importance. Finally, $\Delta E_0=88$ meV and $\Delta E_0=32$ meV were determined from the fits for GaN and ZnO, respectively. Whereas for GaN ΔE_0 is only slightly lower than the LO-phonon energy (see Table III), a large difference between ΔE_0 and $\hbar\omega_{LO}$ values exists for ZnO. This behavior can be understood by considering the polarization cloud in case of ZnO to consist of many multiphonon states. Then, all long-wavelength optical phonons may be assumed to participate in the coupling between the lattice and the excitons. Their mean energy should be between 13 meV (E_2 mode[62–65,124]) and 72 meV (Table III). The observed ΔE_0 value for ZnO falls close to the middle of this interval and is also in excellent agreement with an effec-

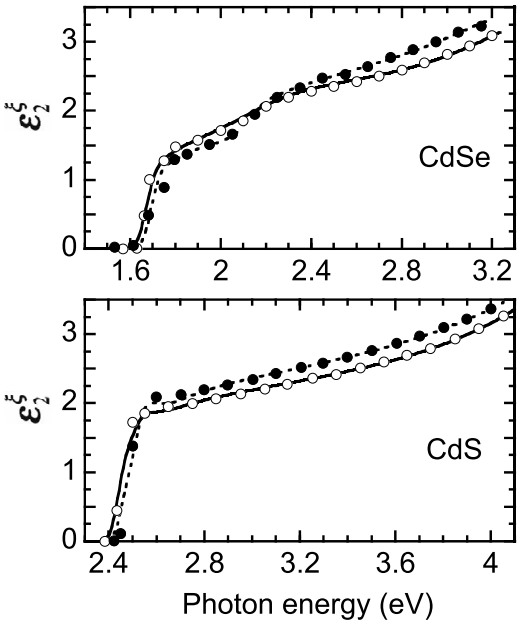

FIG. 7. Experimental ordinary (open circles) and extraordinary (filled circles) DFs of CdS (Ref. 106) and CdSe (Ref. 109) and fits (solid and dotted lines).

tive phonon energy of (33 ± 7) meV which, according to Klingshirn *et al.*,[125] determines the exciton linewidth at not too low temperatures.

Compared with ZnO and GaN, the experimental spectra of the DFs for CdSe and CdS are strongly broadened (see Figs. 6 and 7), and it was impossible to determine unambiguously the EPC parameters for these materials using the above procedure. However, the obtained results for GaN and ZnO demonstrate a correlation between the sum $(\alpha_e+\alpha_h)$ and the b, f_0, and $\Delta E_0/\hbar\omega_{\mathrm{LO}}$ values (see Table III). Therefore, using known $(\alpha_e+\alpha_h)$ values, we estimated the EPC parameters for CdSe and CdS by a linear interpolation between GaN and ZnO. As seen in Table III, the EPC contribution is relatively small for CdSe and CdS compared with ZnO.

VI. RESULTS AND DISCUSSION

In this section, the momentum matrix elements and the CB dispersion relations are reported and discussed. To determine them, calculated ε_2^{ξ} spectra were fitted to experimental ones. Experimental data for the DFs we analyzed are restricted to photon energies of 5.6, 5.2, 4.1, and 3.2 eV for GaN, ZnO, CdS, and CdSe, respectively, which are essentially below their E_1 critical points (approximately 7, 9, 5, and 4 eV, respectively; see e.g., Refs. 1 and 3). In this spectral range, the imaginary part of the DF is determined by excitons at the E_0 critical point and optical transitions between states of the three highest VBs and the lowest CB with electron wave vectors near the zone center. The calculation of ε_2^{ξ} is carried out using Eqs. (1)–(3) and taking into account the EPC contribution, as discussed in Sec. V. Input parameters are given in Tables II and III. The broadening is incorporated into the calculated $\varepsilon_2^{\xi}(E)$ spectra using the Gaussian line-shape function with σ as the broadening parameter. Arguments in favor of the Gaussian broadening as compared to the Lorentzian one have been given previously.[37] Varying the E_P^{ξ} value, coefficients N_i in Eq. (4) and the broadening parameter σ, the calculated ε_2^{ξ} spectrum is adjusted to the experimental one in the whole spectral region studied. The derived CB dispersion relation is then fitted by Eq. (5) to determine the M_j coefficients. Terms up to $i_0=5$ and $j_0=3$ were included in Eqs. (4) and (5), respectively. Since experimental ε_2^{ξ} spectra of ZnO and GaN show features unambiguously identified with discrete excitons, EPC and BB transitions (see Sec. V), the fitting procedure used is capable of determining the m_{e0}^* value. The spectra of CdSe and CdS are rather structureless due to the large broadening of optical transitions (compare Figs. 6 and 7). The determination of m_{e0}^* in a way similar to GaN and ZnO would be unjustified in view of possible correlation between calculated contributions of different mechanisms. Therefore, m_{e0}^* values from cyclotron resonance measurements were used in our calculations for CdSe and CdS (see Sec. II and Table II).

A remark should be made concerning ZnO. Now the anomalous valence-band ordering is mostly accepted (see, e.g., Refs. 20, 86, 126, and 127), which has been explained in terms of a negative spin-orbit splitting.[5,20,126,128] One of the consequences is that the B exciton, not the A, has a larger oscillator strength for the $\mathbf{E}\perp c$ polarization of light.[5] For instance, using RSP parameters of Table II, we obtain $F_{\mathrm{A}\perp}^{\mathrm{DX}}=0.99$ and $F_{\mathrm{B}\perp}^{\mathrm{DX}}=1$. However, the calculated ratio of the oscillator strengths is still close to unity, whereas experiments[5,82,129,130] yield a mean value of about 0.29 for this ratio; i.e., the A exciton is significantly weaker. The discrepancy may be due to the fact that, first, experimental determinations of Δ_i parameters mainly use energy positions of excitons, while oscillator strengths are taken into account only qualitatively; and second, not all important interactions are included into an exciton Hamiltonian used in analyzing experimental data. Gil[131] suggested that, in contrast to GaN, the electron-hole spin exchange interaction is very important for ZnO and including it would account for both the energies and oscillator strengths of excitons even without an inverted VB ordering. Not going into the details of the discussion, we notice that the (A, B) exciton doublet is not resolved at room temperature; hence, we expect little influence of the VB ordering on the DF. However, the experimentally observed weakness of the A exciton means that its contribution to the DF is considerably decreased. In addition, a further experimental observation must be taken into account, namely, the sum of oscillator strengths of A and B excitons in $\mathbf{E}\perp c$ polarization is approximately equal to the oscillator strength of the C exciton in $\mathbf{E}\parallel c$ polarization.[5,82,129,130] Therefore, in calculating the excitonic contribution to the DFs of ZnO, we used the $F_{v\xi}^{\mathrm{DX}}$ values given in Table I which satisfy the above experimental observations. For comparison, the following would result from the RSP parameters listed in Table II: $F_{\mathrm{A}\perp}^{\mathrm{DX}}=0.99$, $F_{\mathrm{B}\perp}^{\mathrm{DX}}=1$, $F_{\mathrm{C}\perp}^{\mathrm{DX}}=0.01$, $F_{\mathrm{A}\parallel}^{\mathrm{DX}}=0.02$, $F_{\mathrm{B}\parallel}^{\mathrm{DX}}=0$, and $F_{\mathrm{C}\parallel}^{\mathrm{DX}}=1.98$. The BB transitions were calculated such as is prescribed by the RSP parameters.

Figures 7 and 8(a) show experimental ε_2^{ξ} spectra (symbols) and fits to them (solid and dotted lines) for CdSe, CdS, and ZnO. From the fits we obtain $E_P^{\perp}$, $E_P^{\parallel}$, N_i, and σ. For GaN, only $\varepsilon_2^{\perp}(E)$ is available from experiment [open circles

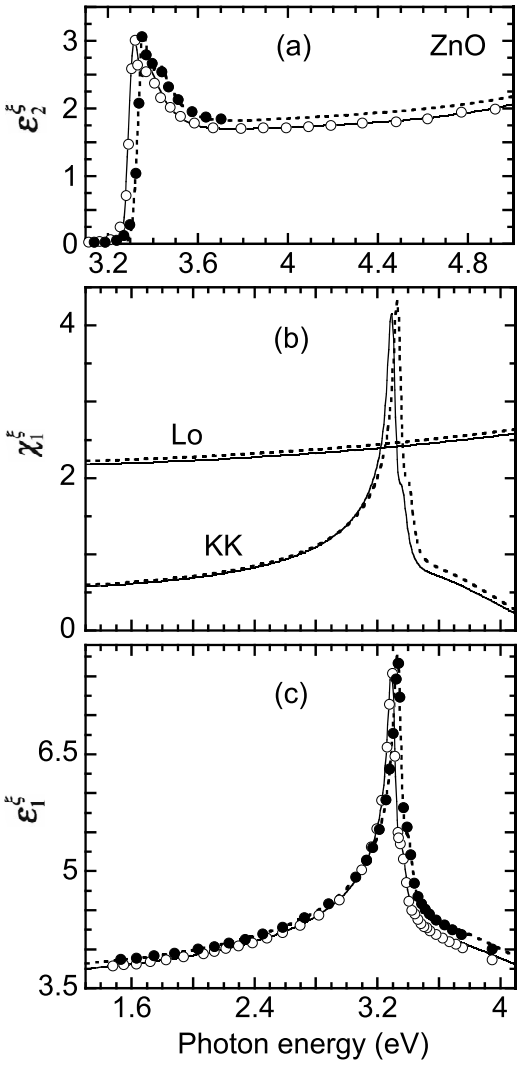

FIG. 8. Measured imaginary (a) and real (c) parts of the ordinary (open circles) and extraordinary (filled circles) DFs of ZnO (Ref. 2 and this work) and fits (solid and dotted lines). (b) Contributions to the real part of the ordinary (solid) and extraordinary (dotted) optical susceptibility due to low-energy and high-energy optical transitions. The lines denoted by KK are obtained by the Kramers-Kronig transformation of the calculated ε_2^ξ spectra of (a). The effect of all high-energy transitions is modeled using a single Lorentz oscillator described by $\chi=B_1/(E_1^2-E^2)$ with the resonance energy $E_1=9.87$ eV and magnitude B_1 to be equal to 208.3 and 212.7 eV^2 for the ordinary and extraordinary waves, respectively.

in Fig. 9(a)]; hence, $E_P^\perp$, N_i, and σ are determined from comparison to the calculation (solid line). Using the derived fitting parameters, $\varepsilon_2^\parallel(E)$ spectrum can be calculated. In Ref. 1, the ratio $\varepsilon_2^\parallel/\varepsilon_2^\perp=1.050$ for photon energies above the E_0 critical point was found from experimental $\varepsilon_1^\perp$ and $\varepsilon_1^\parallel$ in the transparent region. The use of this value as a mean calculated dichroism in the 3.7–4.5 eV spectral region yields an estimate of $E_P^\parallel$. The corresponding $\varepsilon_2^\parallel(E)$ spectrum is shown in Fig. 9(a) by the dotted line.

TABLE IV. Momentum matrix element and its anisotropy.

	GaN	ZnO	CdS	CdSe
$E_P^\perp$ (eV)	18.8	12.8	16.6	22.2
$E_P^\parallel$ (eV)	21.0	14.7	18.7	24.7
$E_P^\parallel/E_P^\perp$	1.117	1.148	1.127	1.113

TABLE V. Nonparabolicity coefficients N_i and M_j [see Eqs. (4) and (5) and text]. k_{lim} and $E_{c,\text{lim}}$ denote the limiting electron wave vector and the energy of their validity, respectively.

	GaN	ZnO	CdS	CdSe
N_1	−2.30	−1.91	−2.80	−3.08
N_2	0.77	0.53	1.09	1.95
N_3	−0.24	−0.48	−0.31	−2.03
N_4	0.07	0.19	0.09	1.05
N_5	0.05	−0.07	−0.007	0.14
k_{lim} (nm^{-1})	4.0	3.8	3.7	3.1
M_1	0.177	0.150	0.246	0.294
M_2	−0.0169	−0.0291	−0.101	−0.203
M_3	0.460	0.0449	0.126	0.209
$E_{c,\text{lim}}$ (eV)	2.0	1.8	1.7	1.6

Results of fits regarding the interband momentum matrix elements and CB dispersion relations are summarized in Tables IV–VI and will be discussed in Secs. VI A and VI C. Note that a similar approach as that in the present work was used by us to study GaN (Ref. 104) and ZnO.[8] However, wave-vector dependence of the BB transition probability and the effect of EPC were neglected in Ref. 104, which resulted in slightly different values of $E_P^\perp$ and m_{e0}^* of GaN compared to this work. For ZnO, we re-examined experimental data for the DFs at higher photon energies (see Sec. IV). The resulting CB dispersion relation differs from that of Ref. 8 as being more realistic, as revealed by analysis in terms of its correspondence to the $\mathbf{k}\cdot\mathbf{p}$ theory (see Sec. VI C).

Now we briefly discuss the relation between dichroism at the E_0 critical point and birefringence in the transparent region and close to the absorption edge. The solid and dotted lines denoted by KK in Fig. 8(b) represent contributions to the real part of the ordinary and extraordinary optical susceptibilities χ of ZnO obtained by the Kramers-Kronig transformation of the respective calculated $\varepsilon_2^\xi(E)$ spectra in Fig. 8(a). Note that the optical susceptibility is related to the DF by $\varepsilon=1+\chi$. Comparison to measured $\varepsilon_1^\xi(E)$ spectra [symbols in Fig. 8(c)] shows that the contribution from the E_0 critical point is not enough to account for the magnitude of the real part of the DFs. This demonstrates an important role of high-energy optical transitions. As shown in Fig. 8(c) by solid and dotted lines, the experimental $\varepsilon_1^\xi(E)$ spectra up to about 3.8 eV can be well described by adding a single nonbroadened Lorentz oscillator. Lines denoted by Lo in Fig. 8(b) represent the resultant contributions of high-energy transitions.

Results of a similar analysis for GaN are illustrated in Figs. 9(b) and 9(c). Experimental $\varepsilon_1^\xi(E)$ data have been reported only for the transparent region [symbols in Fig. 9(c)]. Their values and energy dependence are well accounted for by the above procedure. In addition, we observe that the effects of high-energy critical points on the DFs in the trans-

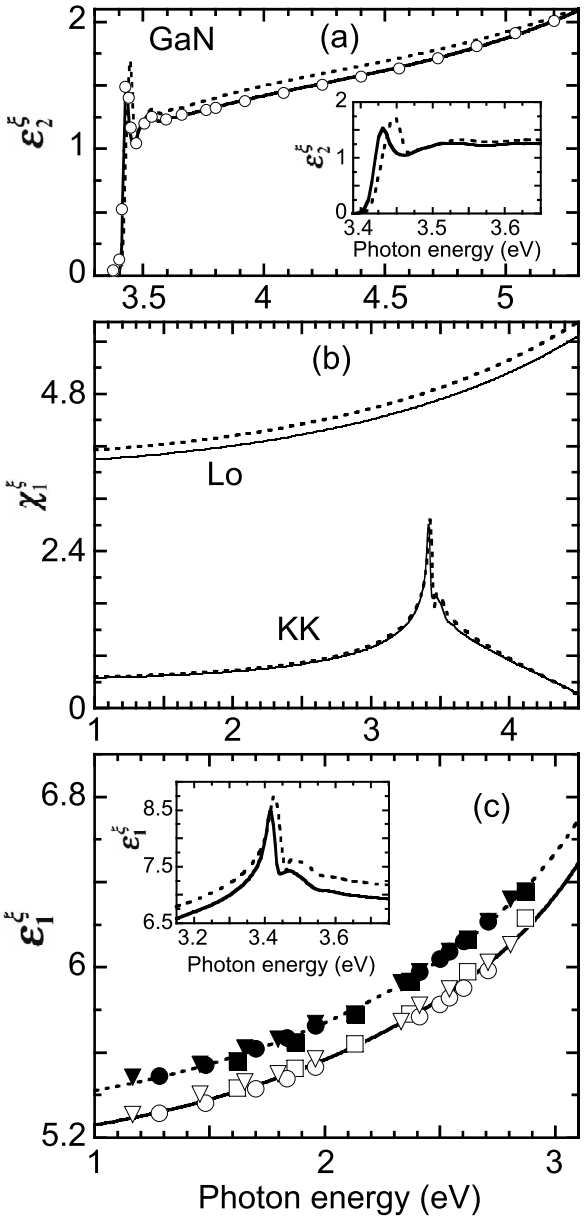

FIG. 9. (a) Experimental $\varepsilon_2^{\perp}(E)$ spectrum of GaN (open circles; Ref. 104) and fit (solid line). The dotted line represents the calculated $\varepsilon_2^{\parallel}(E)$ spectrum, provided $E_P^{\parallel}=21.0$ eV (see text). (b) The same as in Fig. 8(b) but for GaN. $E_1=7.68$ eV; B_1 is equal to 220.4 and 228.8 eV^2 for the ordinary and extraordinary waves, respectively. (c) Measured ε_1^{ξ} (open and filled symbols for ordinary and extraordinary waves, respectively) and fits (solid and dotted lines). The data of Refs. 1, 71, and 132 are denoted by squares, circles, and triangles, respectively. The insets show the calculated ε_2^{ξ} and ε_1^{ξ} spectra close to the absorption edge.

parent region are considerably larger for GaN than for ZnO.

A. Anisotropy of the momentum matrix element

The determined values of the momentum matrix element and its anisotropy, i.e., the ratio $E_P^{\parallel}/E_P^{\perp}$, are listed in Table IV. In the literature, anisotropy of the momentum matrix element was reported only for GaN.[10–12] Rodina and Meyer[10] used experimentally observable anisotropy of the Landé g factor and obtained $E_P^{\perp}=17.7$ eV and $E_P^{\parallel}=18.7$ eV, or $E_P^{\perp}=16.9$ eV and $E_P^{\parallel}=17.8$ eV, dependent on a set of parameters describing the influence of higher conduction bands. The early result by Suzuki and Uenoyama[12] ($E_P^{\perp}=15.4$ eV, $E_P^{\parallel}=13.1$ eV) seems to be not reliable as this was found by fitting the VB energy dispersion calculated under assumption that $\Delta_2=\Delta_3=0$ and $A_7=0$. In addition, $m_{et}<m_{ez}$ was observed in that work, which contradicts most of later calculations (see, e.g., Fig. 4). Rinke *et al.*[11] reported $E_P^{\perp}=16.2$ eV and $E_P^{\parallel}=17.4$ eV from band-structure calculations, which is in qualitative agreement with Ref. 10 and the present work. As seen from Table IV, the anisotropy of the momentum matrix element depends on the semiconductor. Below we shall show that this behavior can be related to the departure of the actual crystal structure from the ideal wurtzite, which is different for the semiconductors in question.

TABLE VI. Band gap E_{gA} and broadening parameter σ derived from fits to experimental ε_2^{ξ} spectra, as well as E_P^* and E^* values that fit the determined conduction-band dispersion relation (see text).

	GaN	ZnO	CdS	CdSe
E_{gA} (eV)	3.451	3.358	2.481	1.681
σ (meV)	6.8	14.5	20	20
E_P^* (eV)	18.6	13.4	13.6	14.5
E^* (eV)	6.11	7.43	4.98	4.46

The ideal wurtzite structure is composed of two interpenetrating hexagonal close-packed sublattices. Each individual sublattice is described by a hexagonal prism with base a and height c. The two sublattices are displaced from each other by a distance $(3/8)^{1/2}a$, and the ratio c/a is $(8/3)^{1/2}\approx 1.633$.[133] Defining a parameter u, such as uc is the relative displacement of the two sublattices, one expects $u=(3/8)=0.375$. Two distortions are possible in the wurtzite structure without destruction of the hexagonal symmetry:[133] the two sublattices may be (a) slightly compressed or dilated along the hexagonal axis and (b) slightly displaced with respect to one another along the hexagonal axis. The distortions would result in changing tetrahedral bond lengths, bond angles, or both, as well as in the departure from the ideal c/a and u values. It is known from experiments that[133–136] only wurtzite structures with c/a ratio lower than the ideal value of 1.633 are stable; the compounds with greatest electronegativity difference have the largest deviation from the ideal c/a, which is explained by long-range polar interactions; the parameter u exceeds the value calculated by $u=[(1/3)(a/c)^2+(1/4)]$, which is expected if the bond lengths would be equal; and a strong correlation between c/a and u exists, i.e., if c/a is decreased then u increases.

From dimensional considerations, Lawaetz[137] and Hermann and Weisbuch[138] concluded that the matrix element of the momentum operator for zinc-blende semiconductors should be inversely proportional to the lattice constant. Another important factor is the ionicity.[137,138] In addition, unequal $E_P^{\perp}$ and $E_P^{\parallel}$ are allowed by the hexagonal symmetry of wurtzite semiconductors.[9] Based on these general results and

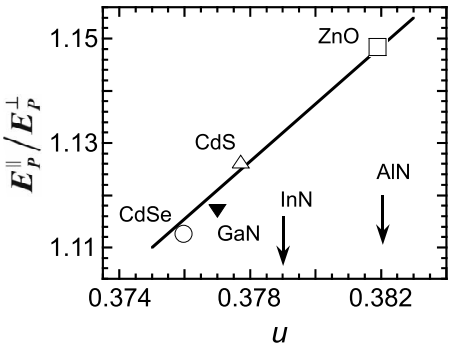

FIG. 10. Anisotropy of the momentum matrix element of CdSe, CdS, ZnO, and GaN as a function of the u parameter of the crystal lattice. The arrows indicate u parameters of InN and AlN.

considering the behavior of actual wurtzite structures described above, the parameter u can be assumed to express the variation in the anisotropy of the momentum matrix element from one compound to the other. Figure 10 shows that such correlation between $E_P^{\parallel}/E_P^{\perp}$ and u is indeed observed for the three II–VI semiconductors studied. The u values were taken from Refs. 139–141 for CdS, CdSe and ZnO, respectively. Extrapolating to $u=0.375$ yields $E_P^{\parallel}/E_P^{\perp} \approx 1.11$. In light of the above discussion, this value may be regarded as an inherent anisotropy of the momentum matrix element for II–VI compounds which would be characteristic of an ideal wurtzite structure. Following Refs. 137 and 138, it can be assumed that the inherent anisotropy is caused by the combined influence of ionicity and interatomic distances within the crystal cell, which is different for directions parallel and perpendicular to the optic axis.

The $E_P^{\parallel}/E_P^{\perp}$ ratio for GaN (filled triangle in Fig. 10) estimated in this work agrees well with data for II–VI semiconductors. The u parameter of GaN was taken from Ref. 136. The arrows indicate u values of InN (Ref. 11) and AlN (Ref. 136). AlN deviates more than GaN and InN from the ideal u; hence, it can be expected that the $E_P^{\parallel}/E_P^{\perp}$ ratio increases along the series GaN, InN, AlN. However, it is not clear whether the anisotropy of the momentum matrix elements of InN and AlN may be quantitatively estimated using the data in Fig. 10 for II–VI semiconductors because III–V semiconductors have a less ionic character. In addition, other factors can play a role, e.g., d electrons[137] or overlap term.[138] Note also that somewhat lower anisotropy was found for GaN in Refs. 10 and 11 from the conduction-band g factor and band-structure calculations (1.055 and 1.074, respectively).

B. Conduction-band dispersion relation and effective mass

The determined CB dispersion relation and effective mass are expressed in terms of the effective mass m_{e0}^* at the CB bottom and nonparabolicity coefficients N_i and M_j [see Eqs. (4) and (5)]. The nonparabolicity coefficients are listed in Table V. When using the coefficients N_i to calculate the CB dispersion relation by Eq. (4), the wave vector should be taken in units of $(\text{Å})^{-1}$, which results in the electron energy in eV.[142] The unit for M_j is $(\text{eV})^{-j}$. To our knowledge, there have been no reports on experimental determination of the

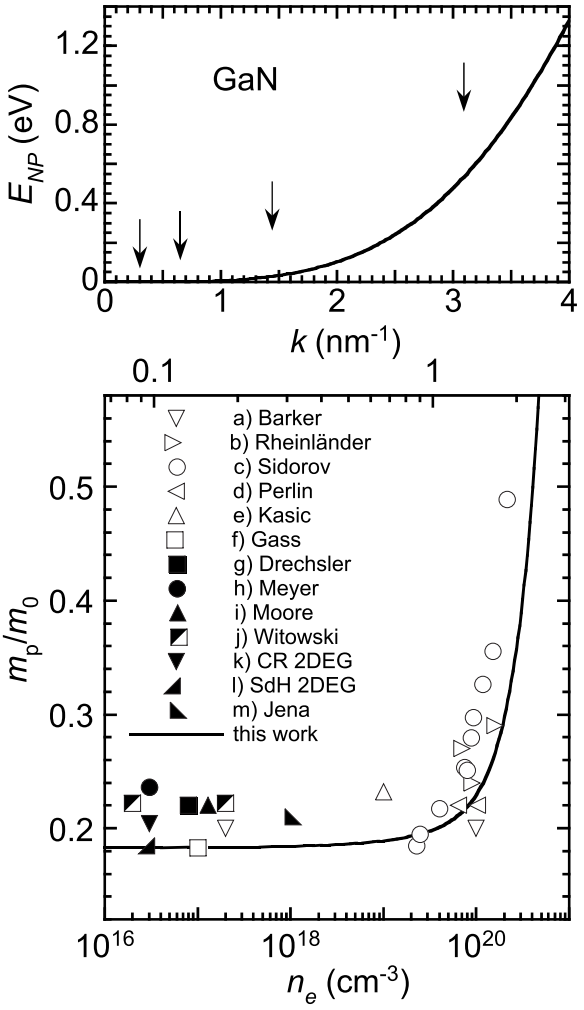

FIG. 11. (Top) Conduction-band nonparabolicity and (bottom) momentum effective mass of GaN determined in this work (solid lines) as a function of wave vector and electron concentration. The arrows indicate wave vectors corresponding to electron concentrations of 10^{18}, 10^{19}, 10^{20}, and 10^{21} cm^{-3} from left to right, respectively. In the bottom panel, the upper x axis relates the wave vector from the top panel with free-electron concentration from the bottom panel. The open and filled symbols denote room-temperature and low-temperature data, respectively, obtained by various experiments (see text). (a) Ref. 66; (b) Ref. 143; (c) Ref. 144; (d) Ref. 145; (e) Ref. 61; (f) Ref. 146; (g) Ref. 147; (h) Ref. 148; (i) Ref. 149; (j) Ref. 150; [(k) and (l)] Ref. 151; (m) Ref. 152.

CB dispersion relation and/or nonparabolicity in the semiconductors in question. Only the electron effective mass has been measured. Using the data in Table V, we calculated the momentum effective mass as a function of electron concentration, as described in Ref. 38, and compared it with existing literature data. We also present the CB nonparabolicity defined as $E_{\text{NP}}=E_{cp}(k)-E_c(k)$, where $E_{cp}(k)$ would be the electron energy for a parabolic band.

Figure 11 represents the results for GaN. The open symbols show room-temperature literature data obtained by infrared reflectance,[66,145] Faraday rotation,[143] thermoelectric power,[144] infrared spectroscopic ellipsometry,[61] and electron energy–loss spectra[146] measurements. Results of low-

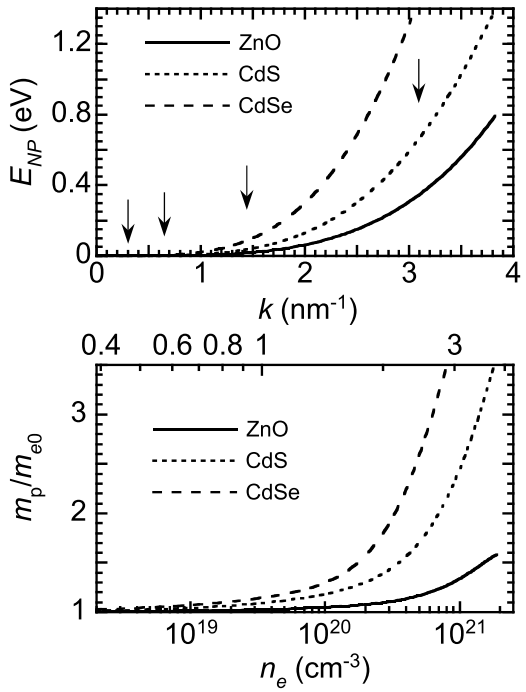

FIG. 12. (Top) Conduction-band nonparabolicity and (bottom) relative momentum effective mass of ZnO, CdS, and CdSe as a function of wave vector and electron concentration. The meaning of arrows in the top panel and the upper x axis in the bottom panel is the same as in Fig. 11.

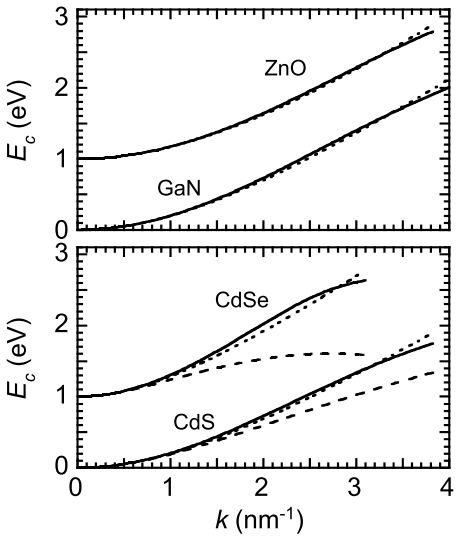

FIG. 13. The determined conduction-band dispersion relations (solid) and fits (dotted) by Eqs. (10) and (11). The dashed lines show the calculated result for CdS and CdSe, provided E_P^* is taken to be 17.7 and 23.5 eV, respectively (see text for more details). For clarity, the curves for ZnO and CdSe are shifted vertically by 1 eV.

temperature cyclotron resonance study[147] and far-infrared spectroscopy of shallow donors[148–150] are shown by filled symbols. Also included are mean values of the effective mass at the band edge deduced from low-temperature cyclotron resonance and Shubnikov–de Haas experiments with structures containing a two-dimensional electron gas (see Ref. 151), as well as the electron effective mass from Shubnikov–de Haas oscillations in a polarization-doped three-dimensional electron slab in a graded $Al_xGa_{1-x}N$ layer.[152] Generally, there is good agreement between our data and literature data regarding the dependence on the electron concentration, although some uncertainty remains concerning the exact m_{e0}^* value. Note, however, that due to localization effects, the measured low-temperature effective mass may be somewhat overestimated by experiments such as infrared spectroscopy of shallow donors or trapped electron cyclotron resonance which is usually observed in wide-gap semiconductors.[153]

The CB nonparabolicities and relative momentum effective masses of ZnO, CdS, and CdSe are presented in Fig. 12 as a function of electron concentration and wave vector. To our knowledge, there have been no experimental studies of free-carrier effects on the electron effective mass in these compounds. The m_{e0}^* value of 0.216 we determined in this work for ZnO (see Table II) is in good agreement with recent calculations[20,27] but is slightly lower than those derived from infrared reflectance[154] (0.265), Faraday effect[155] (0.24), and cyclotron resonance[35,49] (0.26 and 0.265).

The arrows in Figs. 11 and 12 indicate wave vectors (electron energies) which would correspond to several electron concentrations from 10^{18} up to 10^{21} cm^{-3}. It can be concluded that the method we used provides experimental determination of the CB structure up to electron energies significantly higher than those achievable by conventional doping.

C. Comparison to k·p models

Now the obtained results will be analyzed in terms of their correspondence to the **k·p** theory. In this discussion, we closely follow Ref. 38 and will not repeat details concerning models of the CB structure. Following Ruf and Cardona,[156] who employed an effective two-band model to describe the nonparabolicity of the CB in GaAs, we define the spin-orbit-crystal-field-averaged fundamental gap E_0^* of a wurtzite semiconductor by $E_0^*=(1/3)(E_{gA}+E_{gB}+E_{gC})$. In terms of Δ_i energies, this reads $E_0^*=E_{gA}+(1/3)(\Delta_1+3\Delta_2)$. Then the CB dispersion relation and the effective mass at the CB bottom are expressed as follows:

$$E_c(k) = -\frac{E_0^*}{2} + \frac{E_0^*}{2}\left[1 + \frac{\hbar^2 k^2}{2m_0}\frac{4E_P^*}{(E_0^*)^2}\right]^{1/2} + \frac{\hbar^2 k^2}{2m_0}(1 + C^*), \tag{10}$$

$$1/m_{e0}^* = 1 + E_P^*/E_0^* + C^* \tag{11}$$

where the momentum matrix element is denoted by E_P^* and the C^* parameter accounts for effects of higher conduction bands and remote bands.[138,156] One should expect that the E_P^* value is approximately equal to the average of $E_P^\perp$ and $E_P^\parallel$.

Considering the averaged band gap and the electron effective mass at the band edge to be known, we have two unknowns in Eqs. (10) and (11), E_P^* and C^*, and, hence, only one adjusted parameter, E_P^*, for instance, to fit the determined CB dispersion relation by Eq. (10). The fits are shown in Fig. 13, while the resultant E_P^* values are listed in Table VI. For

more clarity, curves for ZnO and CdSe in Fig. 13 are shifted upward by 1 eV. As can be seen, Eq. (10) provides a satisfactory description of the CB dispersion. However, one has to anticipate the systematic deviation from experiment due to incapability of Eq. (10) to reproduce to the full extent the transition from the quadratic into sublinear dependence as k is increased.

Comparing Tables IV and VI, we see that the deduced E_P^*'s for GaN and ZnO are close to the corresponding E_P^ξ's, which demonstrates the self-consistency of different parameters determined in the present study for these two materials. For CdS and CdSe, there is a considerable discrepancy between the E_P^* and E_P^ξ values. The average of $E_P^\perp$ and $E_P^\parallel$ is 17.7 and 23.5 eV for CdS and CdSe, respectively. Using it as the value of E_P^* in Eq. (11) yields the C^* parameter. Then the CB dispersions can be calculated by Eq. (10). The result is shown in Fig. 13 (bottom) by dashed lines, which deviate considerably from experiment. This indicates that the E_P^ξ values for CdS and CdSe are somewhat high, implying that the ε_2^ξ magnitude is probably overestimated in Refs. 106 and 109 due to the neglect of surface effects.

Within the framework of a simple model of the CB structure given by $\hbar^2k^2/(2m_0m_{e0}^*)=E_c(1+E_c/E^*)$, the constant E^* can immediately be interpreted as a measure of the CB nonparabolicity.[38] E^* values, for which the above equation matches the determined CB dispersion relation at $k=k_0$, where the wave vector k_0 corresponds to an electron concentration of 2×10^{19} cm^{-3}, are listed in Table VI. They are considerably larger than the band-gap energies. This means that, generally, the conduction band of wurtzite semiconductors is less nonparabolic as compared to most zinc-blende compounds.[38] A similar behavior is also observed for zinc-blende GaN, CdS, and CdSe.[38]

VII. SUMMARY

We studied the dichroism of wurtzite semiconductors in the vicinity of the E_0 critical point. The method we used is based upon comparing the calculated imaginary parts of the ordinary and extraordinary DFs with experiment. Contributions from discrete excitons, band-to-band transitions, and EPCs were included. The valence-band structure and transition probability were calculated within the framework of the 6×6 Rashba-Sheka-Pikus Hamiltonian. The CB was assumed to be spherical. According to the results we presented, the interband matrix elements $E_P^\parallel$ and $E_P^\perp$ of the momentum operator along and perpendicular to the optic axis, respectively, are different, with $E_P^\parallel$ exceeding $E_P^\perp$ and the $E_P^\parallel/E_P^\perp$ ratio increasing along the series CdSe, CdS, ZnO. The u parameters of GaN, InN, and AlN suggest that the $E_P^\parallel/E_P^\perp$ ratio should increase along the GaN, InN, AlN series as well. The determined anisotropy of the momentum matrix element was interpreted in terms of an inherent anisotropy that would be characteristic of an ideal wurtzite structure and the departure of the actual crystal structure from the ideal wurtzite, which is individual for each semiconductor.

We also determined the CB dispersion relation and nonparabolicity, as well as effective mass, as a function of electron concentration and wave vector for GaN, ZnO, CdS, and CdSe. Analysis of the derived parameters in terms of correspondence to the $\mathbf{k}\cdot\mathbf{p}$ theory showed that those of GaN and ZnO are self-consistent, while $E_P^\parallel$ and $E_P^\perp$ values for CdS and CdSe are somewhat high, which, probably, is due to the neglected surface effects in Refs. 106 and 109.

In addition, optical response due to transitions into EPC was observed and analyzed. We found that the EPC effects in ZnO are in the same order as those due to free excitons. It follows from the proposed model that states with up to about ten phonons may be effective in processes when a photon simultaneously creates an exciton and several phonons. For GaN, the EPC contribution to the optical response is of less importance compared to ZnO.

ACKNOWLEDGMENTS

This work was supported by the Deutsche Forschungsgemeinschaft (Grants No. GO 586/6-1, No. AM 105/5-1, and No. ME 898/24-1).

*Corresponding author; sviatoslav.shokhovets@tu-ilmenau.de

[1] S. Shokhovets, R. Goldhahn, G. Gobsch, S. Piekh, R. Lantier, A. Rizzi, V. Lebedev, and W. Richter, J. Appl. Phys. **94**, 307 (2003).
[2] G. E. Jellison, Jr. and L. A. Boatner, Phys. Rev. B **58**, 3586 (1998); S.S. thanks G. E. Jellison for providing original data for the DFs of ZnO and helpful discussions regarding generalized ellipsometry.
[3] S. Adachi, *Optical Constants of Crystalline and Amorphous Semiconductors: Numerical Data and Graphical Information* (Kluwer, Boston, 1999).
[4] J. L. Birman, Phys. Rev. **114**, 1490 (1959).
[5] D. G. Thomas, J. Phys. Chem. Solids **15**, 86 (1960); J. J. Hopfield, *ibid.* **15**, 97 (1960).
[6] K. Kim, W. R. L. Lambrecht, B. Segall, and M. van Schilfgaarde, Phys. Rev. B **56**, 7363 (1997).
[7] Y. M. Sirenko, J. B. Jeon, B. C. Lee, K. W. Kim, M. A. Littlejohn, M. A. Stroscio, and G. J. Iafrate, Phys. Rev. B **55**, 4360 (1997).
[8] S. Shokhovets, G. Gobsch, and O. Ambacher, Superlattices Microstruct. **39**, 299 (2006).
[9] G. L. Bir and G. E. Pikus, *Symmetry and Strain-Induced Effects in Semiconductors* (Wiley, New York, 1974).
[10] A. V. Rodina and B. K. Meyer, Phys. Rev. B **64**, 245209 (2001).
[11] P. Rinke, M. Scheffler, A. Qteish, M. Winkelnkemper, D. Bimberg, and J. Neugebauer, Appl. Phys. Lett. **89**, 161919 (2006).
[12] M. Suzuki and T. Uenoyama, Jpn. J. Appl. Phys., Part 1 **35**, 543 (1996).
[13] M. Suzuki, T. Uenoyama, and A. Yanase, Phys. Rev. B **52**, 8132 (1995); *Properties, Processing and Applications of Gallium Nitride and Related Semiconductors*, edited by J. H. Edgar, S. Strite, I. Akasaki, H. Amano, and C. Wetzel (INSPEC, IEE, Lon-

don, 1999), pp. 168–182.
[14] J.-B. Jeon, Yu. M. Sirenko, K. W. Kim, M. A. Littlejohn, and M. A. Stroscio, Solid State Commun. **99**, 423 (1996).
[15] J. A. Majewski, M. Städele, and P. Vogl, in *III-V Nitrides*, MRS Symposia Proceedings No. 449 (Materials Research Society, Pittsburgh, 1996), p. 887.
[16] Y. C. Yeo, T. C. Chong, and M. F. Li, J. Appl. Phys. **83**, 1429 (1998).
[17] G. B. Ren, Y. M. Liu, and P. Blood, Appl. Phys. Lett. **74**, 1117 (1999).
[18] D. J. Dugdale, S. Brand, and R. A. Abram, Phys. Rev. B **61**, 12933 (2000).
[19] D. Fritsch, H. Schmidt, and M. Grundmann, Phys. Rev. B **67**, 235205 (2003).
[20] W. R. L. Lambrecht, A. V. Rodina, S. Limpijumnong, B. Segall, and B. K. Meyer, Phys. Rev. B **65**, 075207 (2002).
[21] W. F. Fan, J. B. Xia, P. A. Agus, S. T. Tan, S. F. Yu, and X. W. Sun, J. Appl. Phys. **99**, 013702 (2006).
[22] Y.-N. Xu and W. Y. Ching, Phys. Rev. B **48**, 4335 (1993).
[23] K. Miwa and A. Fukumoto, Phys. Rev. B **48**, 7897 (1993).
[24] M. Goano, E. Bellotti, E. Ghillino, G. Ghione, and K. F. Brennan, J. Appl. Phys. **88**, 6487 (2000).
[25] C. Persson, Bo E. Semelius, A. Ferreira da Silva, C. Moysés Araújo, R. Ahuja, and B. Johansson, J. Appl. Phys. **92**, 3207 (2002).
[26] P. Carrier and S.-H. Wei, J. Appl. Phys. **97**, 033707 (2005).
[27] M. Oshikiri, F. Aryasetiawan, Y. Imanaka, and G. Kido, Phys. Rev. B **66**, 125204 (2002).
[28] G. D. Chen, M. Smith, J. Y. Lin, H. X. Jiang, S.-H. Wei, M. Asif Khan, and C. J. Sun, Appl. Phys. Lett. **68**, 2784 (1996).
[29] S. K. Pugh, D. J. Dugdale, S. Brand, and R. A. Abram, Semicond. Sci. Technol. **14**, 23 (1999).
[30] T. Yang, S. Nakjima, and S. Sakai, Jpn. J. Appl. Phys., Part 1 **34**, 5912 (1995).
[31] B. Jogai, Solid State Commun. **107**, 345 (1998).
[32] J.-B. Xia, K. W. Cheah, X.-L. Wang, D.-Z. Sun, and M.-Y. Kong, Phys. Rev. B **59**, 10119 (1999).
[33] I. Vurgaftman and J. R. Meyer, J. Appl. Phys. **94**, 3675 (2003).
[34] *Numerical Data and Functional Relationships in Science and Technology*, Landolt-Börnstein, New Series, Group III, Vol. 41, Pt. B, edited by O. Madelung, U. Rössler, and M. Schulz (Springer, Berlin, 1999).
[35] K. Y. Button, D. R. Cohn, M. von Ortenbert, B. Lax, E. Mollwo, and R. Helbig, Phys. Rev. Lett. **28**, 1637 (1972).
[36] E. F. Venger, A. V. Melnichuk, L. Yu. Melnichuk, and Yu. A. Pasechnik, Phys. Status Solidi B **188**, 823 (1995).
[37] S. Shokhovets, G. Gobsch, and O. Ambacher, Phys. Rev. B **74**, 155209 (2006).
[38] S. Shokhovets, O. Ambacher, and G. Gobsch, Phys. Rev. B **76**, 125203 (2007).
[39] J. J. Hopfield and D. G. Thomas, Phys. Rev. **122**, 35 (1961).
[40] B. L. Evans, in *Physics and Chemistry of Materials with Layered Structures*, edited by P. A. Lee (Reidel, Holland, 1976), Vol. 4, p. 1.
[41] E. A. Muljarov, A. L. Yablonskii, S. G. Tikhodeev, A. E. Bulatov, and J. L. Birman, Phys. Rev. B **59**, 4600 (1999).
[42] A. V. Rodina, M. Dietrich, A. Göldner, L. Eckey, A. Hoffmann, Al. L. Efros, M. Rosen, and B. K. Meyer, Phys. Rev. B **64**, 115204 (2001).
[43] D. W. Langer, R. N. Euwema, K. Era, and T. Koda, Phys. Rev. B **2**, 4005 (1970).
[44] J.-M. Wagner and F. Bechstedt, Phys. Rev. B **66**, 115202 (2002).
[45] A. A. Yamaguchi, Y. Mochizuki, H. Sunakawa, and A. Usui, J. Appl. Phys. **83**, 4542 (1998).
[46] K. Torii, T. Deguchi, T. Sota, K. Suzuki, S. Chichibu, and S. Nakamura, Phys. Rev. B **60**, 4723 (1999).
[47] B. Gil, in *Semiconductors and Semimetals*, edited by J. I. Pankove and T. D. Moustakas (Academic, San Diego, 1999), Vol. 57, p. 209, and references therein.
[48] K. Kornitzer, T. Ebner, M. Grehl, K. Thonke, R. Sauer, C. Kirchner, V. Schwegler, M. Kamp, M. Leszczynski, I. Grzegory, and S. Porowski, Phys. Status Solidi B **216**, 5 (1999).
[49] Y. Imanaka, T. Takamusu, K. Takehana, M. Oshikiri, G. Kido, H. Nojiri, Y. H. Matsuda, H. Arimoto, S. Takeyama, N. Miura, G. Karczewski, T. Wojtowicz, and J. Kossut, Phys. Status Solidi B **243**, 939 (2006).
[50] C. A. Arguello, D. L. Rousseau, and S. P. S. Porto, Phys. Rev. **181**, 1351 (1969).
[51] W. I. Bond, J. Appl. Phys. **36**, 1674 (1965).
[52] M. P. Lisitsa, L. F. Gudymenko, V. N. Melinko, and S. F. Terekhova, Phys. Status Solidi **31**, 389 (1969).
[53] A. N. Pikhtin and A. D. Yas'kov, Fiz. Tekh. Poluprovodn. (S.-Peterburg) **15**, 15 (1981); Sov. Phys. Semicond. **15**, 8 (1981).
[54] T. Kozawa, T. Kachi, H. Kano, Y. Taga, M. Hashimoto, N. Koide, and K. Manabe, J. Appl. Phys. **75**, 1098 (1994).
[55] T. Azuhata, T. Sota, K. Suzuki, and S. Nakamura, J. Phys.: Condens. Matter **7**, L129 (1995).
[56] H. Siegle, L. Eckey, A. Hoffmann, C. Thomsen, B. K. Meyer, D. Shikora, M. Hankeln, and K. Lischka, Solid State Commun. **96**, 943 (1995).
[57] V. Yu. Davydov, Yu. E. Kitaev, I. N. Goncharuk, A. N. Smirnov, J. Graul, O. Semchinova, D. Uffmann, M. B. Smirnov, A. P. Mirgorodsky, and R. A. Evarestov, Phys. Rev. B **58**, 12899 (1998).
[58] T. Deguchi, D. Ichiryu, K. Toshikawa, K. Sekiguchi, T. Sota, R. Matsuo, T. Azuhata, M. Yamaguchi, T. Yagi, S. Chichibu, and S. Nakamura, J. Appl. Phys. **86**, 1860 (1999).
[59] A. R. Goñi, H. Siegle, K. Syassen, C. Thomsen, and J.-M. Wagner, Phys. Rev. B **64**, 035205 (2001).
[60] G. Mirjalili, T. Dumelow, T. J. Parker, S. Fajami Shayesteh, T. S. Cheng, C. T. Foxon, L. C. Jenkins, and D. E. Lacklinson, Infrared Phys. Technol. **37**, 389 (1996).
[61] A. Kasic, M. Schubert, S. Einfeldt, D. Hommel, and T. E. Tiwald, Phys. Rev. B **62**, 7365 (2000).
[62] T. C. Damen, S. P. S. Porto, and B. Tell, Phys. Rev. **142**, 570 (1966).
[63] B. H. Bairamov, A. Heinrich, G. Irmer, V. V. Toporov, and E. Ziegler, Phys. Status Solidi B **119**, 227 (1983).
[64] F. Decremps, J. Pellicer-Porres, A. M. Saitta, J. C. Chervin, and A. Polian, Phys. Rev. B **65**, 092101 (2002).
[65] N. Ashkenov, B. N. Mbenkum, C. Bundesmann, V. Riede, M. Lorenz, D. Spemann, E. M. Kaidashev, A. Kasic, M. Shubert, M. Grundmann, G. Wagner, H. Neumann, V. Darakchieva, H. Arwin, and B. Monemar, J. Appl. Phys. **93**, 126 (2003).
[66] A. S. Barker, Jr. and M. Ilegems, Phys. Rev. B **7**, 743 (1973).
[67] E. C. Heltemes and H. L. Swinney, J. Appl. Phys. **38**, 2387 (1967).
[68] H. W. Verleur and A. S. Barker, Jr., Phys. Rev. **155**, 750 (1967).
[69] A. S. Barker, Jr. and C. J. Summers, J. Appl. Phys. **41**, 3552 (1970).

[70] R. Geick, C. H. Perry, and S. S. Mitra, J. Appl. Phys. **37**, 1994 (1966).
[71] M. J. Bergmann, Ü. Özgür, H. C. Casey, Jr., H. O. Everitt, and J. F. Muth, Appl. Phys. Lett. **75**, 67 (1999).
[72] C. W. Teng, J. F. Muth, Ü. Özgür, M. J. Bergmann, H. O. Everitt, A. K. Sharma, C. Jin, and J. Narayan, Appl. Phys. Lett. **76**, 979 (2000).
[73] H. Yoshikawa and S. Adachi, Jpn. J. Appl. Phys., Part 1 **36**, 6237 (1997).
[74] W. Shan, B. D. Little, A. J. Fischer, J. J. Song, B. Goldenberg, W. G. Perry, M. D. Bremser, and R. F. Davis, Phys. Rev. B **54**, 16369 (1996).
[75] M. Steube, K. Reimann, D. Fröhlich, and S. J. Clarke, Appl. Phys. Lett. **71**, 948 (1997).
[76] S. Tripathy, R. K. Soni, H. Asahi, K. Iwata, R. Kuroiwa, K. Asami, and S. Gonda, J. Appl. Phys. **85**, 8386 (1999).
[77] K. Kornitzer, T. Ebner, K. Thonke, R. Sauer, C. Kirchner, V. Schwegler, M. Kamp, M. Leszczynski, I. Grzegory, and S. Porowski, Phys. Rev. B **60**, 1471 (1999).
[78] W. Y. Liang and A. D. Yoffe, Phys. Rev. Lett. **20**, 59 (1968).
[79] A. Mang, K. Reimann, and St. Rübenacke, Solid State Commun. **94**, 251 (1995).
[80] D. C. Reynolds, D. C. Look, B. Jogai, C. W. Litton, G. Cantwell, and W. C. Harsch, Phys. Rev. B **60**, 2340 (1999).
[81] S. Ozaki, T. Mishima, and S. Adachi, Jpn. J. Appl. Phys., Part 1 **42**, 5465 (2003).
[82] S. F. Chichibu, T. Sota, G. Cantwell, D. B. Eason, and C. W. Litton, J. Appl. Phys. **93**, 756 (2003).
[83] D. C. Reynolds, C. W. Litton, D. C. Look, J. E. Hoelscher, B. Claflin, T. C. Collins, J. Nause, and B. Nemeth, J. Appl. Phys. **95**, 4802 (2004).
[84] W. Shan, W. Walukiewicz, J. W. Ager III, K. M. Yu, H. B. Yuan, H. P. Xin, G. Cantwell, and J. J. Song, Appl. Phys. Lett. **86**, 191911 (2005).
[85] R. Laskowski, N. E. Christensen, G. Santi, and C. Ambrosch-Draxl, Phys. Rev. B **72**, 035204 (2005).
[86] R. Laskowski and N. E. Christensen, Phys. Rev. B **73**, 045201 (2006).
[87] D. Volm, K. Oettinger, T. Streibl, D. Kovalev, M. Ben-Chorin, J. Diener, B. K. Meyer, J. Majewski, L. Eckey, A. Hoffmann, H. Amano, I. Akasaki, K. Hiramatsu, and T. Detchprohm, Phys. Rev. B **53**, 16543 (1996).
[88] B. J. Skromme, J. Jayapalan, R. P. Vaudo, and V. M. Phanse, Appl. Phys. Lett. **74**, 2358 (1999).
[89] Y. S. Park, C. W. Litton, T. C. Collins, and D. C. Reynolds, Phys. Rev. **143**, 512 (1966).
[90] C. W. Litton, D. C. Reynolds, and T. C. Collins, Phys. Rev. B **6**, 2269 (1972).
[91] A. Imada, S. Ozaki, and S. Adachi, J. Appl. Phys. **92**, 1793 (2002).
[92] I. Strzalkowski, S. Joshi, and C. R. Crowell, Appl. Phys. Lett. **28**, 350 (1976).
[93] I. B. Kobiakov, Solid State Commun. **35**, 305 (1980).
[94] G. A. Samara, Phys. Rev. B **27**, 3494 (1983).
[95] M. Schall, M. Walther, and P. U. Jepsen, Phys. Rev. B **64**, 094301 (2001).
[96] A. Polian, M. Grimsditch, and I. Grzegory, J. Appl. Phys. **79**, 3343 (1996).
[97] A. Jeżowski, B. A. Danilchenko, M. Boćkowski, I. Grzegory, S. Krukowski, T. Suski, and T. Paszkiewicz, Solid State Commun. **128**, 69 (2003).
[98] R. K. Kremer, M. Cardona, E. Schmitt, J. Blumm, S. K. Estreicher, M. Sanati, M. Bockowski, I. Grzegory, T. Suski, and A. Jezowski, Phys. Rev. B **72**, 075209 (2005).
[99] Y. Oshima, T. Suzuki, T. Eri, Y. Kawaguchi, K. Watanabe, M. Shibata, and T. Mishima, J. Appl. Phys. **98**, 103509 (2005).
[100] B. A. Danilchenko, T. Paszkiewicz, S. Wolski, A. Jeżowski, and T. Plackowski, Appl. Phys. Lett. **89**, 061901 (2006).
[101] C. Mion, J. F. Muth, E. A. Preble, and D. Hanser, Appl. Phys. Lett. **89**, 092123 (2006).
[102] S. L. Chuang and C. S. Chang, Phys. Rev. B **54**, 2491 (1996).
[103] S. Shokhovets, G. Goldhahn, V. Cimalla, T. S. Cheng, and C. T. Foxon, J. Appl. Phys. **84**, 1561 (1998); G. Goldhahn and S. Shokhovets, in *III-Nitride Semiconductors: Optical Properties II*, edited by M. O. Manasreh and H. X. Jiang (Taylor & Francis, New York, 2002), p. 73.
[104] S. Shokhovets, G. Gobsch, and O. Ambacher, Appl. Phys. Lett. **86**, 161908 (2005).
[105] Ph. Hofmann, K. Horn, A. M. Bradshaw, R. L. Johnson, D. Fuchs, and M. Cardona, Phys. Rev. B **47**, 1639 (1993).
[106] S. Ninomiya and S. Adachi, J. Appl. Phys. **78**, 1183 (1995); see, also Ref. 3.
[107] S. Logothetidis, M. Cardona, P. Lautenschläger, and M. Garriga, Phys. Rev. B **34**, 2458 (1986).
[108] C. Janowitz, O. Günther, G. Jungk, R. L. Johnson, P. V. Santos, M. Cardona, W. Faschinger, and H. Sitter, Phys. Rev. B **50**, 2181 (1994).
[109] S. Ninomiya and S. Adachi, J. Appl. Phys. **78**, 4681 (1995); see, also Ref. 3.
[110] A. J. Fischer, W. Shan, J. J. Song, Y. C. Chang, R. Horning, and B. Goldenberg, Appl. Phys. Lett. **71**, 1981 (1997).
[111] J. F. Muth, J. H. Lee, I. K. Shmagin, R. M. Kolbas, H. C. Casey, Jr., B. P. Keller, U. K. Mishra, and S. P. DenBaars, Appl. Phys. Lett. **71**, 2572 (1997).
[112] J. F. Muth, R. M. Kolbas, A. K. Sharma, S. Oktyabrsky, and J. Narayan, J. Appl. Phys. **85**, 7884 (1999).
[113] P. L. Washington, H. C. Ong, J. Y. Dai, and R. P. H. Chang, Appl. Phys. Lett. **72**, 3261 (1998).
[114] J. Dillinger, Č. Koňák, V. Prosser, J. Sak, and M. Zvára, Phys. Status Solidi **29**, 707 (1968).
[115] C. F. Klingshirn, *Semiconductor Optics* (Springer, Berlin, 1997).
[116] R. Zimmermann and C. Trallero-Giner, Phys. Rev. B **56**, 9488 (1997).
[117] Y. Toyozawa and J. Hermanson, Phys. Rev. Lett. **21**, 1637 (1968); J. Hermanson, Phys. Rev. B **2**, 5043 (1970).
[118] J. Sak, Phys. Rev. Lett. **25**, 1654 (1970).
[119] K. Hannewald and P. A. Bobbert, Phys. Rev. B **72**, 113202 (2005).
[120] T. D. Lee, F. E. Low, and D. Pines, Phys. Rev. **90**, 297 (1953).
[121] J. Pollmann and H. Büttner, Phys. Rev. B **16**, 4480 (1977).
[122] U. Rössler and H.-R. Trebin, Phys. Rev. B **23**, 1961 (1981).
[123] A. S. Mishchenko, N. V. Prokofev, A. Sakamoto, and B. V. Svistunov, Phys. Rev. B **62**, 6317 (2000).
[124] K. Hazu, T. Sota, S. Adachi, Sf. Chichibu, G. Cantwell, D. C. Reynolds, and C. W. Litton, J. Appl. Phys. **96**, 1270 (2004).
[125] C. Klingshirn, R. Hauschild, J. Fallert, and H. Kalt, Phys. Rev. B **75**, 115203 (2007).
[126] L. C. Lew Yan Voon, M. Willatzen, M. Cardona, and N. E. Christensen, Phys. Rev. B **53**, 10703 (1996).
[127] A. V. Rodina, M. Strassburg, M. Dworzak, U. Haboeck, A. Hoff-

mann, A. Zeuner, H. R. Alves, D. M. Hofmann, and B. K. Meyer, Phys. Rev. B **69**, 125206 (2004).
[128] J. E. Rowe, M. Cardona, and F. H. Pollak, Solid State Commun. **6**, 239 (1968).
[129] M. Zamfirescu, A. Kavokin, B. Gil, G. Malpuech, and M. Kaliteevski, Phys. Rev. B **65**, 161205(R) (2002).
[130] S. Tsoi, X. Lu, A. K. Ramdas, H. Alawadhi, M. Grimsditch, M. Cardona, and R. Lauck, Phys. Rev. B **74**, 165203 (2006).
[131] B. Gil, Phys. Rev. B **64**, 201310(R) (2001); J. Appl. Phys. **98**, 086114 (2005).
[132] N. A. Sanford, L. H. Robins, A. V. Davydov, A. Shapiro, D. V. Tsvetkov, A. V. Dmitriev, S. Keller, U. K. Mishra, and S. P. DenBaars, J. Appl. Phys. **94**, 2980 (2003).
[133] G. A. Jeffrey, G. S. Parry, and R. L. Mozzi, J. Chem. Phys. **25**, 1024 (1956); F. Keffer and A. M. Portis, *ibid.* **27**, 675 (1957).
[134] N. N. Sirota, A. I. Olekhnovich, and N. M. Olekhnovich, Acta Crystallogr., Sect. A: Cryst. Phys., Diffr., Theor. Gen. Crystallogr. **24**, 639 (1968).
[135] E. H. Kisi and M. M. Elcombe, Acta Crystallogr., Sect. C: Cryst. Struct. Commun. **45**, 1867 (1989).
[136] H. Schulz and K. H. Thiemann, Solid State Commun. **23**, 815 (1977).
[137] P. Lawaetz, Phys. Rev. B **4**, 3460 (1971).
[138] C. Hermann and C. Weisbuch, Phys. Rev. B **15**, 823 (1977).
[139] A. W. Stevenson, M. Milanko, and Z. Barnea, Acta Crystallogr., Sect. B: Struct. Sci. **40**, 521 (1984).
[140] A. W. Stevenson and Z. Barnea, Acta Crystallogr., Sect. B: Struct. Sci. **40**, 530 (1984).
[141] H. Karzel, W. Potzel, M. Köfferlein, W. Schiessl, M. Steiner, U. Hiller, G. M. Kalvius, D. W. Mitchell, T. P. Das, P. Blaha, K. Schwarz, and M. P. Pasternak, Phys. Rev. B **53**, 11425 (1996).
[142] The same is valid for Ni coefficients in Ref. 38. Note the unit error in the caption to Table II of Ref. 38. The correct unit is $eV(Å)^{2(i+1)}$.
[143] B. Rheinländer and H. Neumann, Phys. Status Solidi B **64**, K123 (1974).
[144] V. G. Sidorov, L. S. Sveshkova, M. D. Shagalov, and Yu. Shalabutov, Fiz. Tekh. Poluprovodn. (S.-Peterburg) **10**, 2200 (1976); Sov. Phys. Semicond. **10**, 1309 (1977).
[145] P. Perlin, E. Litwin-Staszewska, B. Suchanek, W. Knap, J. Camassel, T. Suski, R. Piotrzkowski, I. Grzegory, S. Porowski, and J. C. Chervin, Appl. Phys. Lett. **68**, 1114 (1996).
[146] M. H. Gass, A. J. Papworth, R. Beanland, T. J. Bullough, and P. R. Chalker, Phys. Rev. B **73**, 035312 (2006).
[147] M. Drechsler, D. M. Hofmann, B. K. Meyer, T. Detchprohm, H. Amano, and I. Akasaki, Jpn. J. Appl. Phys., Part 2 **34**, L1178 (1995).
[148] B. K. Meyer, D. Volm, A. Graber, H. C. Alt, T. Detchprohm, H. Amano, and I. Akasaki, Solid State Commun. **95**, 597 (1995).
[149] W. J. Moore, J. A. Freitas, Jr., and R. J. Molnar, Phys. Rev. B **56**, 12073 (1997).
[150] A. M. Witowski, K. Pakula, J. M. Baranowski, M. L. Sadowski, and P. Wyder, Appl. Phys. Lett. **75**, 4154 (1999).
[151] S. Syed, J. B. Heroux, Y. J. Wang, M. J. Manfra, R. J. Molnar, and H. L. Stormer, Appl. Phys. Lett. **83**, 4553 (2003).
[152] D. Jena, S. Heikman, J. S. Speck, A. Gossard, U. K. Mishra, A. Link, and O. Ambacher, Phys. Rev. B **67**, 153306 (2003).
[153] Y. Imanaka, M. Oshikiri, K. Takehana, T. Takamusu, and G. Kido, Physica B (Amsterdam) **298**, 211 (2001).
[154] R. L. Weiher, Phys. Rev. **152**, 736 (1966).
[155] W. S. Baer, Phys. Rev. **154**, 785 (1967).
[156] T. Ruf and M. Cardona, Phys. Rev. B **41**, 10747 (1990).